U.S. Department
of Transportation
National Highway
Traffic Safety
Administration

NHTSA

DOT HS 813 836 September 2026

Variability Study for 50th Percentile Females and Males

This page is intentionally left blank.

DISCLAIMER

Suggested APA Format Citation:

Hu, J., Lin, Y-.S., Boyle, K., Khandare, S., Bonifas, A., Reed, M.P. (2026, September). *Variability study for 50th percentile females and males* (Report No. DOT HS 813 836). National Highway Traffic Safety Administration. https://doi.org/10.21949/ed4c-5z72

This page is intentionally left blank.

Technical Report Documentation Page

1. Report No. DOT HS 813 836	**2. Government Accession No.**	**3. Recipient's Catalog No.**
4. Title and Subtitle Variability Study for 50th Percentile Females and Males		**5. Report Date** September 2026 **6. Performing Organization Code**
7. Authors Jingwen Hu, Yang-Shen Lin, Kyle Boyle, Sujata Khandare, Anne Bonifas, Matthew P. Reed		**8. Performing Organization Report No.** UMTRI 2026
9. Performing Organization Name and Address University of Michigan Transportation Research Institute 2901 Baxter Rd, Ann Arbor, MI 48109		**10. Work Unit No.** **11. Contract or Grant No.** 693JJ921D000021/693JJ923F000251
12. Sponsoring Agency Name and Address National Highway Traffic Safety Administration 1200 New Jersey Avenue SE Washington, DC 20590		**13. Type of Report and Period Covered** Final **14. Sponsoring Agency Code** NSR-220

15. Supplementary Notes

The authors would like to acknowledge Global Human Body Modeling Consortium on the human body models.
Digital Object Identifier: https://doi.org/10.21949/ed4c-5z72

16. Abstract

The objective of this research is to use parametric human body models (HBMs) to understand how geometric variability among individuals who have the same sex, stature, and body weight may affect the impact responses and injury outcomes, focusing on the midsize male and midsize female populations.

We first detailed the methods of quantifying the geometric variations in skeleton and external body surface in midsize male and midsize female occupants using principal component analysis, regression, and residual error analysis. Our findings revealed significant geometric variability in the ribcage and pelvis, whereas variations in the femur and tibia were minimal for both midsize males and females.

Based on these geometric analyses, nine midsize male and nine midsize female geometry models were developed, focusing on ribcage and pelvis variations, which account for the majority of the observed geometric variability. The simplified GHBMC midsize male model was then anatomically adjusted (morphed) to match the predicted geometries of the 18 HBMs.

Subsequently, 162 impact simulations were conducted under nine impact conditions using the morphed HBMs. Overall, the component-level impact simulations demonstrated relatively small variations in HBM impact responses among models with the same sex, stature, and body weight. However, in the U.S. New Car Assessment Program frontal crash simulations, notable variations in injury risk were observed, especially in the front passenger position. These results suggest that geometric variability, even among HBMs with the same sex, stature, and body weight, should not be overlooked when assessing injury risks in severe frontal crashes.

17. Key Words human body model, virtual testing, model validation, crash simulations, injury assessment		**18. Distribution Statement** Document is available to the public from the DOT, BTS, National Transportation Library, Repository & Open Science Access Portal, https://rosap.ntl.bts.gov.	
19. Security Classif. (of this report)	**20. Security Classif. (of this page)**	**21. No. of Pages** 58	**22. Price**

Form DOT F 1700.7 (8-72) Reproduction of completed page authorized

This page is intentionally left blank.

Table of Contents

List of Figures

List of Tables

Background

Human Body Models and Their Limitations on Geometric Variations

Finite element (FE) human body models (HBMs) have advanced significantly over the past decade as an important tool for assessing occupant injury risks in motor-vehicle crashes. The continued development of THUMS (Total Human Model for Safety) and GHBMC (Global Human Body Modeling Consortium) models has enhanced the capability and accuracy of FE HBMs in injury assessment. Both model families include several sizes (5th percentile female, 50th and 95th percentile male for THUMS, and 5th and 50th percentile female, 50th and 95th percentile male for GHBMC) of adults in seated posture. These HBMs are valuable research tools for studying occupant injury mechanisms and assessing detailed injury outcomes in motor-vehicle crashes, but they represent only a small amount of the variance in human body size and shape. Specifically, each of them was developed based on the geometry from a single subject. Therefore, models with the same reference stature and weight contain substantially different geometry in other aspects such as the skeleton and external body surface. In addition, although models with various adult body sizes are available, they do not account for the additional geometric variations (effects of age, sitting height, obesity, and body fat percentage) other than those used to select the subjects.

Figure 1 shows the geometry comparison between the THUMS and GHBMC 50th percentile male models by matching their hip location and eye fore-aft location. Although these two models share the same nominal stature and body weight, the GHBMC model has a longer torso, longer cervical spine, wider pelvis, and deeper ribcage than the THUMS model. This comparison highlights the human geometry variation in the so-called "50th percentile male" population and poses the question of how such geometry variations may affect simulated injury outcomes.

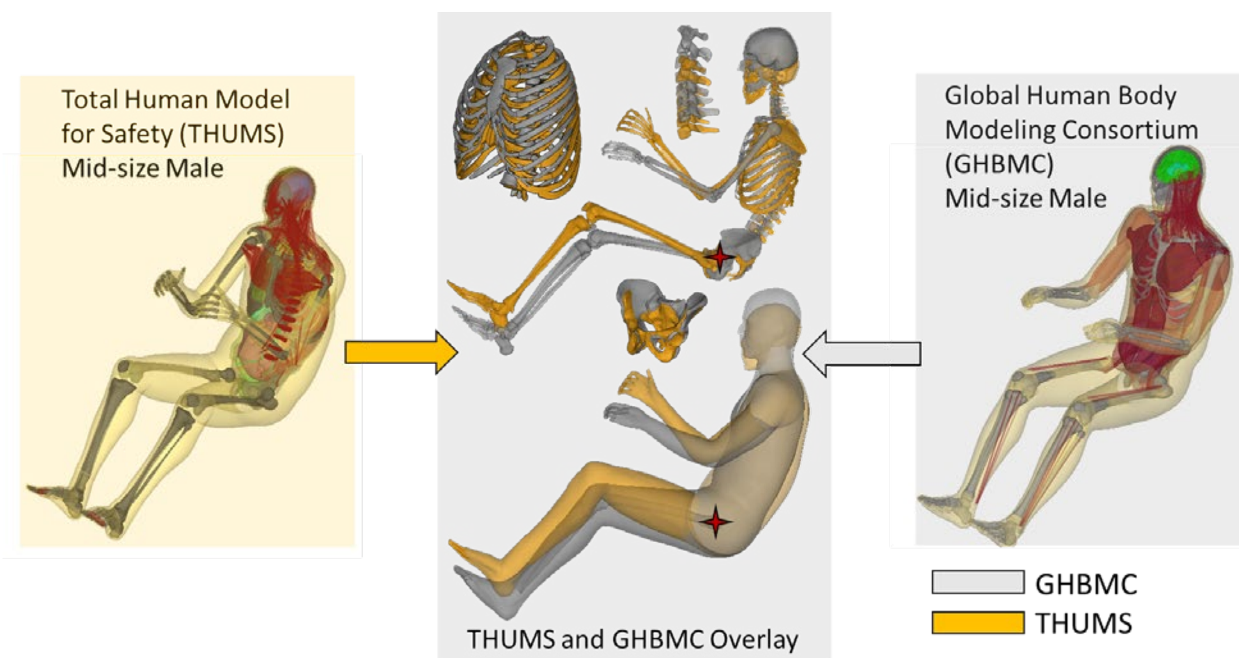

Figure 1. Geometry comparison between THUMS and GHBMC 50th percentile male models

“50th Percentile Males” and “50th Percentile Females” Are NOT Well-Defined Populations

Anthropomorphic test devices (ATDs) and HBMs are often referred to using the “percentile” nomenclature, starting with the so-called “50th percentile male.” Conceptually, an ATD could be constructed that had 50th percentile values on all dimensions for some population. No human matches this body size on more than a few dimensions, but the parts can be assembled to create a whole that is plausible. For example, adding 50th percentile lower extremity lengths to a 50th percentile male torso results in a total body length at the 50th percentile. However, no actual person is “50th percentile,” and the number of people with more than a few dimensions near the 50th percentile is small. This fact was first documented in the 1950s by a U.S. Air Force researcher who conducted a fruitless search for the “average man” (Daniels, 1952).

We have repeated the analysis by Daniels (1952) using data from U.S. Army’s “ANSUR2” survey from 2012. Table 1 shows the search for a “50th percentile male” among 4,083 men. We first filtered on stature, then filtered on sitting height with the remaining men, and so on to the right in the table. If the range from 45th to 55th percentile is considered “50th percentile,” then after filtering on four variables, only a single individual is left. Broadening the criteria to the central 40 percent leaves only 2.2 percent after only four variables. Even using loose definitions of these “percentile people,” we find that “50th percentile males” do not exist in any meaningful way. Although these findings flow directly from the commonsense observation that humans are not simply scaled versions of each other, the implications for anthropometric measurement and modeling are not broadly understood. It is not meaningful to consider “50th percentile males” or “50th percentile females” as actual populations of individuals who can be sampled. In this study, we recognize this by focusing on the residual that remains after sampling “50th percentile” male or female occupants from the entire population.

Table 1. Counts (percentages) from a population of 4,083 men using various quantile criteria, filtering left to right on four anthropometric variables

Total Subjects	Quantile Criterion	Subjects After Filtering Variables Using Quantile Criterion			
		Stature	Stature + Sitting Height	Stature + Sitting Height + Buttock-Knee Length	Stature + Sitting Height + Buttock-Knee Length + Knee Height
4,083 (100%)	0.45 – 0.55	392 (10%)	32 (0.8%)	3 (0.07%)	1 (0.02%)
4,083 (100%)	0.4 – 0.6	774 (19%)	140 (3.4%)	23 (0.6%)	5 (0.1%)
4,083 (100%)	0.3 – 0.7	1616 (40%)	631 (15.5%)	247 (6%)	91 (2.2%)

Research Objective

The overall objective of this research is to use parametric HBMs to understand how geometric variability among individuals who have the same sex, stature, and body weight may affect the injury outcomes. Three specific tasks were conducted.

- Task 1: Measure and analyze geometry data for midsize women and men
- Task 2: Morph HBMs into varied geometry targets to account for the geometric variations among midsize women and men
- Task 3: Conduct impact simulations to quantify the effects from geometric variations on injury outcomes

This page is intentionally left blank.

Task 1: Measure and Analyze Data for Midsize Female and Male

The goal of this task is to statistically quantify the geometric variability of skeleton and external body shape for U.S. occupants who have the same sex, stature, and body weight. To do so, we followed well-established principles on body size descriptions, sampling methods, and variability quantifications.

Human Geometry Data and Statistical Human Geometry Models

Over the past decade, a set of detailed statistical geometry models that include major components of the human skeleton, as well as the external body surface, has been developed. Although the method for developing statistical models of different bones and external body surface varies somewhat between studies, the general approach typically involves four steps, as shown in Figure 2. First, clinical CT scans or 3D body laser scans are obtained using a protocol approved by an institutional review board (IRB) at the University of Michigan to ensure human data acquisition is conducted in accordance with all Federal, institutional, and ethical guidelines. A radiologist reviews CT scans to ensure no abnormality exists in the anatomical regions of interest. Second, geometry data is extracted from images or body surface scans, which includes image processing and segmentation, data cleaning, landmark identification, and template mesh mapping. The goal of the data extraction is to obtain a homologous set of landmarks/mesh on every subject to define the skeleton or external body shape geometry. Because landmarks at corresponding locations should be identified in all the sampled subjects, this step can be time-consuming, although semi-automated methods have been developed in recent studies. Third, a series of statistical analyses are performed to develop the predictive geometry model. These methods include generalized procrustes alignment, principal component analysis (PCA), and multivariate regression analysis. Lastly, a set of coefficient matrices can represent the final statistical model. With any given set of subject covariates, including age, sex, stature, sitting height/stature, and body mass index (BMI), the landmark locations or the nodal coordinates of the template mesh can be predicted.

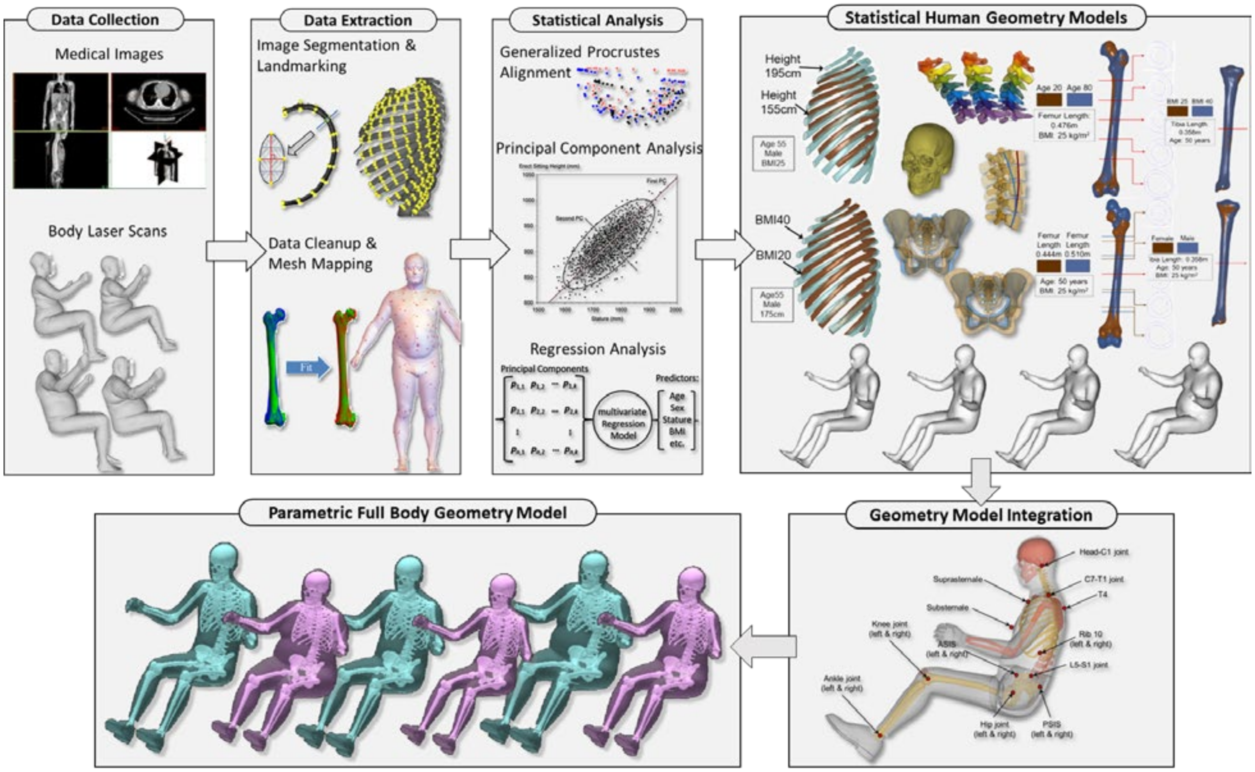

Figure 2. Statistical human geometry model methodology

Table 2 provides the subject sample size and publications for the current versions of the statistical geometry models available for use in this study. For each study, the sampled subjects cover a range of age, stature, and BMI for male and female U.S. adults. To integrate the skeleton model and the external body shape model together, bony landmarks collected from the body scan data are used to position each bone into the body surface model, while local mesh morphing is performed to correct potential bone-to-skin penetrations and bone-to-bone interactions.[1] With any given set of subject covariates (sex, age, stature, SHS, and BMI) for an adult, the skeleton and body shape geometry can be predicted. This suite of statistical body geometry models serves as the foundation of this study to investigate the geometric variations that remain after accounting for sex, stature, and body weight.

Table 2. Publications on statistical human geometry models

Body Region	Sex	Subject Number	Data	References
External Surface	F	73	3D body scan	(Park et al., 2022)
	M	82		
Pelvis	F	75	CT	(Brynskog et al., 2021)
	M	57		
Femur	F	36	CT	(Klein et al., 2015)
	M	62		
Tibia	F	28	CT	(Klein, 2015)

[1]A demonstration version of the fully integrated full body human geometry HERMES model is available at http://humanshape.org/HERMES/MDP_web_public/HERMES_geometry_model.

Body Region	Sex	Subject Number	Data	References
	M	48		
Ribcage	F	47	CT	(Wang et al., 2016) Recently updated
	M	54		
Cervical-Spine	F	79	CT and X-ray	(Reed and Jones, 2017)
	M	61		
Lumbar-Spine	F	82	CT	(Tang et al., 2022)
	M			
Skull	F	54	CT	(Wei et al., 2022)
	M	47		

Further CT Data Analysis Focusing on Ribcage Geometry for Midsize Female and Male

As shown in Table 2, the current statistical human geometry models cover most bones that are associated with major injuries in motor-vehicle crashes. In this study, we further increased the sample size for the ribcage model, specifically with more subjects close to the 50th percentile male-female target values. We focused on the ribcage, because the GHBMC simplified model that was morphed in the following tasks defines all bones as rigid bodies except for the ribcage. As a result, the geometry variations in the ribcage have the most important effects on HBM impact responses. In addition, serious chest injuries, i.e., abbreviated injury scale 3 and higher (AIS3+) chest injuries, are the most common serious injuries in the field.

In this study, we collected high-resolution chest CT scans from 279 subjects with 0.625 mm slice distance following a protocol approved by an IRB at the University of Michigan. Among the 279 subjects, more than 50 percent were between 25th and 75th percentile values of either the stature or the weight. We analyzed all CT scans with subject height or weight between 25th and 75th percentile values using a similar protocol used in our previous study (Wang et al., 2016), although more recently developed mesh mapping and non-rigid registration functions were used to increase the efficiency of data extraction. Specifically, we first leveraged an AI-based CT segmentation tool “TotalSegmentator” to segment ribcage and thoracic spine; then Mimics, a 3D medical image analysis software, was used to improve the segmentation quality for each subject; and finally a template mesh was mapped onto the segmented ribcage geometry through 3D non-rigid registration and iterative mesh morphing methods.[2] The extracted new subject data were used for statistical analyses. Demographic distribution of the newly sampled subjects and an example of the automatic method using TotalSegmentator, Mimics, and mesh mapping are shown in Figure 3 and Figure 4.

[2] Materialise, Leuven, Belgium. https://www.materialise.com

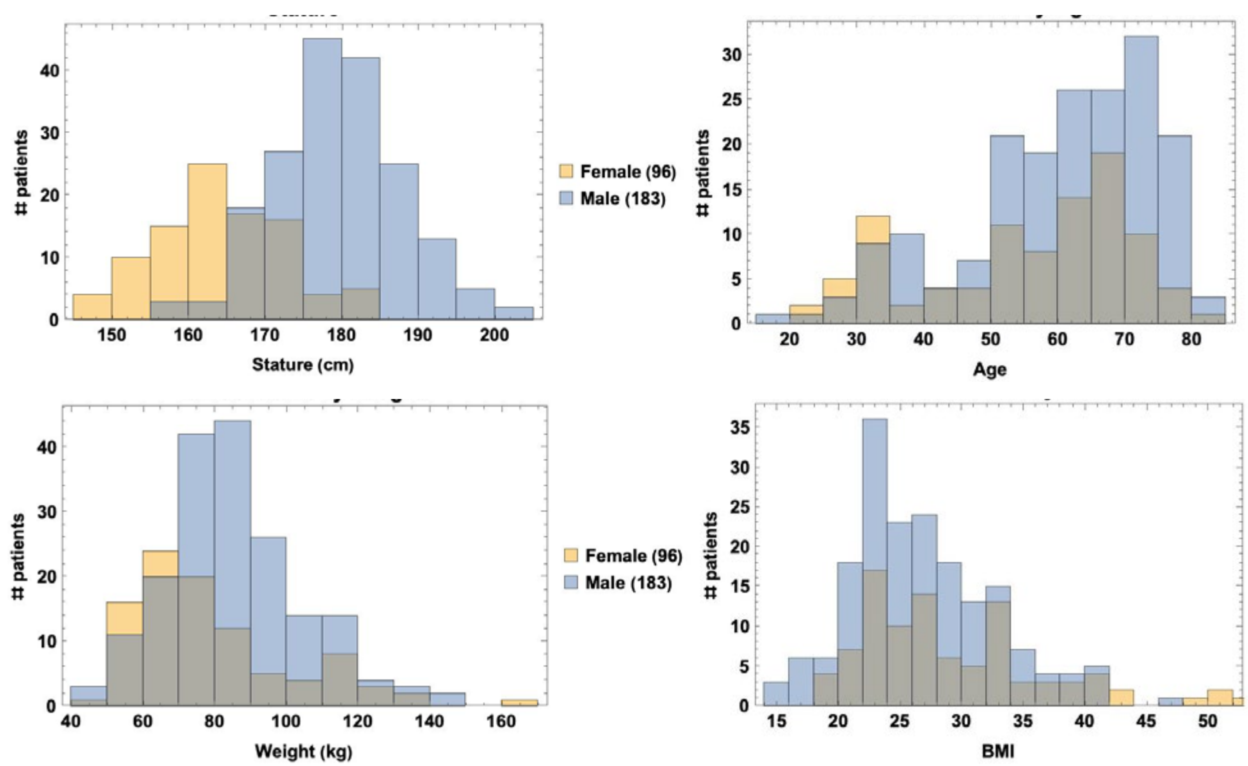

Figure 3. Demographic distribution of the newly collected CT scans

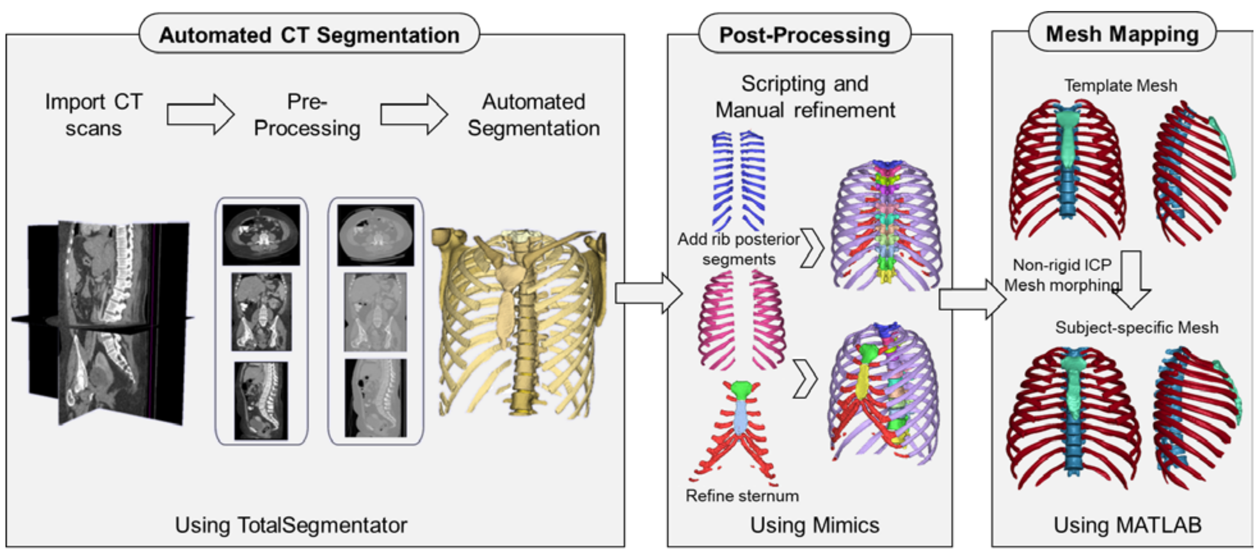

Figure 4. An example of automatic method to achieve homologous ribcage mesh from CT scans

Residual Error Quantifications for the Bone and Body Shape Geometries for Midsize Female and Male

The PCA and regression analysis for generating statistical bone geometry models have been well documented in our previous publications in Table 2. In this process, PCA is used to express the geometry data on an orthogonal basis that can be more readily analyzed and to quantify the data variance in a more efficient way. Geometrically, the first PC is the direction in the space of the data with the highest variance in the nodal coordinates, the second PC is in the direction orthogonal to the first PC with the second highest variance, and so on. Multivariate regression analysis is used to predict how the PC scores associated with each PC may vary with age, sex, height, BMI, and other subject covariates, and in turn predict detailed human body geometry. This is the common practice in our previous studies. However, in this study, the goal is to quantify the geometric variations with the same stature and weight.

Equations 1 and 2 describe the process of calculating residual errors in the geometry data. Assume that geometry data were collected for *n* subjects and each subject geometry was represented by *N* nodes. Equation 1 describes the PCA that rearranges the subject data into the multiplication of PC scores and PC coefficients, where the subject data is represented by coordinates (*x, y, z*) for each node of each subject, and PC scores for each subject are represented by *Sij*, with *i* being the subject number and *j* being the number of PC.

$$\begin{matrix}\text{Subject 1}\\ \vdots \\ \text{Subject n}\end{matrix}\;\underbrace{\begin{bmatrix} x_{11} & \cdots & z_{1N}\\ \vdots & \ddots & \vdots \\ x_{n1} & \cdots & z_{nN}\end{bmatrix}_{n\times 3N}}_{\text{Subject data}} = \overset{\text{PC1}\;\cdots\;\text{PCn}}{\underbrace{\begin{bmatrix} s_{11} & \cdots & s_{1n}\\ \vdots & \ddots & \vdots \\ s_{n1} & \cdots & s_{nn}\end{bmatrix}_{n\times n}}_{\text{PC Scores}}} \times \underbrace{\begin{bmatrix} PC_{11} & \cdots & PC_{1N}\\ \vdots & \ddots & \vdots \\ PC_{n1} & \cdots & PC_{nN}\end{bmatrix}_{n\times 3N}}_{\text{PC Coefficients}} \quad (1)$$

Then the subject covariates (e.g., age, sex, stature, BMI, etc.) were used to predict the PC scores for each subject through multivariate regressions, and the resulted regression coefficients (*Cij*) were used in Equation 2 to calculate residual errors. Through Equation 2, the residual error for each PC of each subject *i* can be calculated.

$$\begin{matrix}\text{PC1}\\ \vdots \\ \text{PCn}\end{matrix}\;\underset{\substack{\text{Residual Errors}\\ \text{of subject } i}}{\begin{bmatrix} ResErr_{i1}\\ \vdots \\ ResErr_{in}\end{bmatrix}_{n\times 1}} = \underset{\substack{\text{PC Scores}\\ \text{of subject } i}}{\begin{bmatrix} s_{i1}\\ \vdots \\ s_{in}\end{bmatrix}_{n\times 1}} - \underbrace{\begin{bmatrix} c_{11} & \cdots & c_{15}\\ \vdots & \ddots & \vdots \\ c_{n1} & \cdots & c_{n5}\end{bmatrix}_{n\times 5}}_{\text{Regression Coefficients}} \times \underbrace{[Age_i, Sex_i, Stature_i, BMI_i, 1]_{5\times 1}}_{\text{Subject } i \text{ covariates}}{}^{T} \quad (2)$$

Note that the subject covariates may vary depending on the body regions.

The residual errors for all the sampled subjects were evaluated to ensure that no strong correlation exists between the residual errors and any subject covariate. If a strong correlation does exist, the predictors, i.e., subject covariates, used for the regression model need to be adjusted into different forms. The residual errors for the top PCs (typically PC1 and PC2) were then further evaluated to check whether they significantly affect the geometry. If yes, a second PCA was conducted for the residual errors in the top two PCs, and an ellipse was generated based on the PC scores and chi-square values to cover 95 percent of the residual error variations with the center at the average midsize male and midsize female locations. Subjects at the vertices/co-vertices of the major and minor axes of the ellipse were then selected for both midsize males and midsize females to demonstrate the geometric variations. The same residual error analysis was conducted for the ribcage, pelvis, femur, tibia, and the external body surface.

Ribcage Geometry Residual Errors

Figure 5 shows the percentage of total variance explained by each PC (left) and the PC residual errors in male and female subjects (right) for the ribcage geometry model. The first two PCs dominated the variance by accounting for over 65 percent of the total geometric variance in the ribcage. The residual errors are also distributed wider in the first two PCs compared to the rest PCs. A higher residual error suggests that subject covariates have limited predictive power for the associated PC score, which leads to greater variation in the predicted geometry in the PC direction.

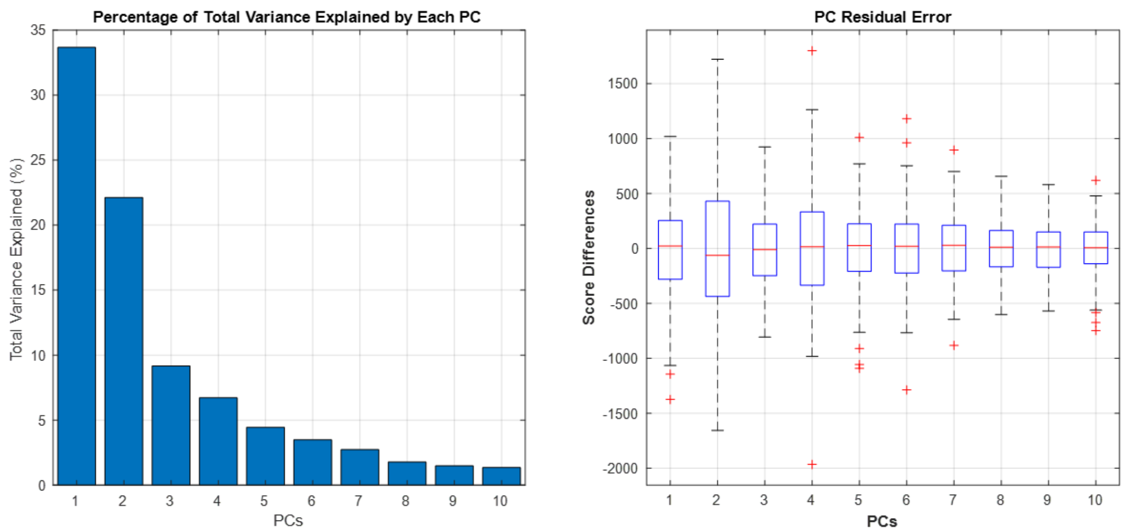

Figure 5. PCA and residual error results for the ribcage geometry model

Figure 6 shows the residual error distributions for PC1 and PC2 with respect to subject torso height, BMI, and age, and the 3D ribcage geometry with the 5th, 50th, and 95th residual errors for midsize male. The residual errors do not have any strong correlations to the subject covariates, meaning that any specific subject shares the same residual errors as the male or female population. The residual errors in PC1 show clear effects on the ribcage depth and rib angles, while the residual errors in PC2 show considerable effects on ribcage shape, especially the bottom half of the ribcage as shown in Figure 6.

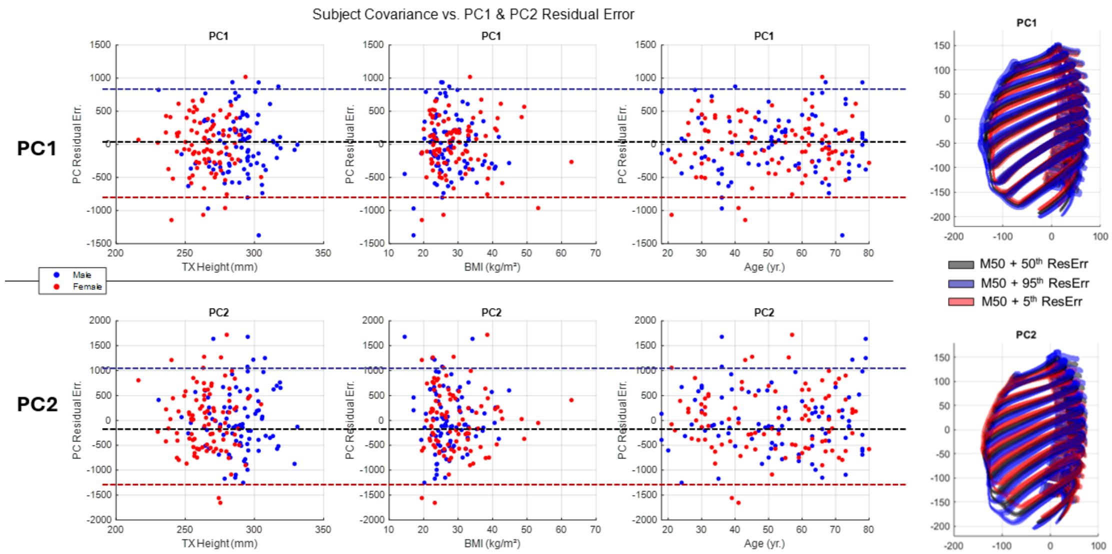

Figure 6. Ribcage first two PC residual error distributions and effects

Figure 7 shows five ribcage geometries for midsize males and five for midsize females. The black color represents the average midsize male or midsize female, respectively. The four blue ribcage and four red ribcage geometries are at the vertices/co-vertices of the major and minor axes of the ellipse that covers 95 percent of the residual errors for males and females, respectively. These ribcages show clear shape variations in the midsize male and female populations.

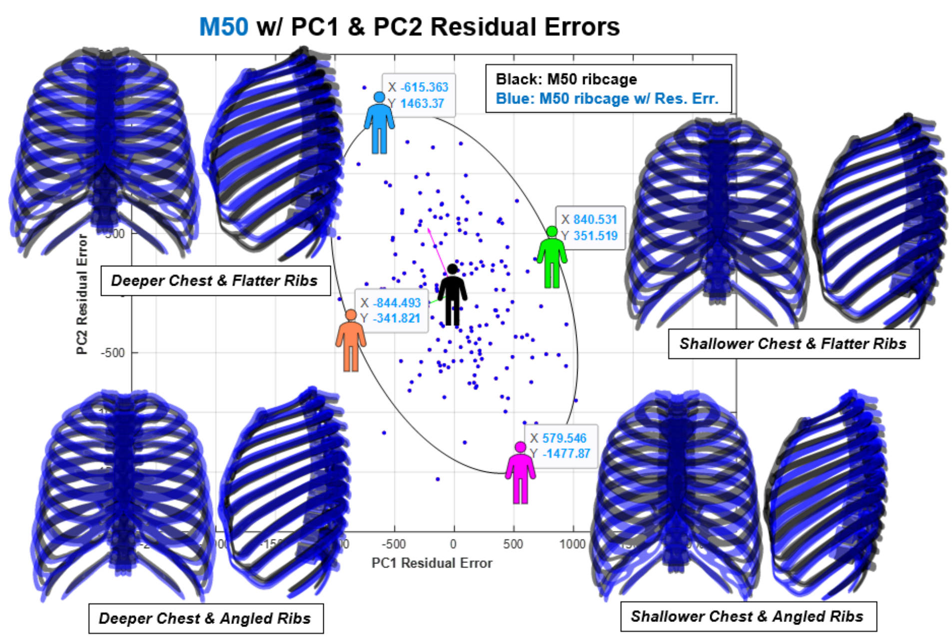

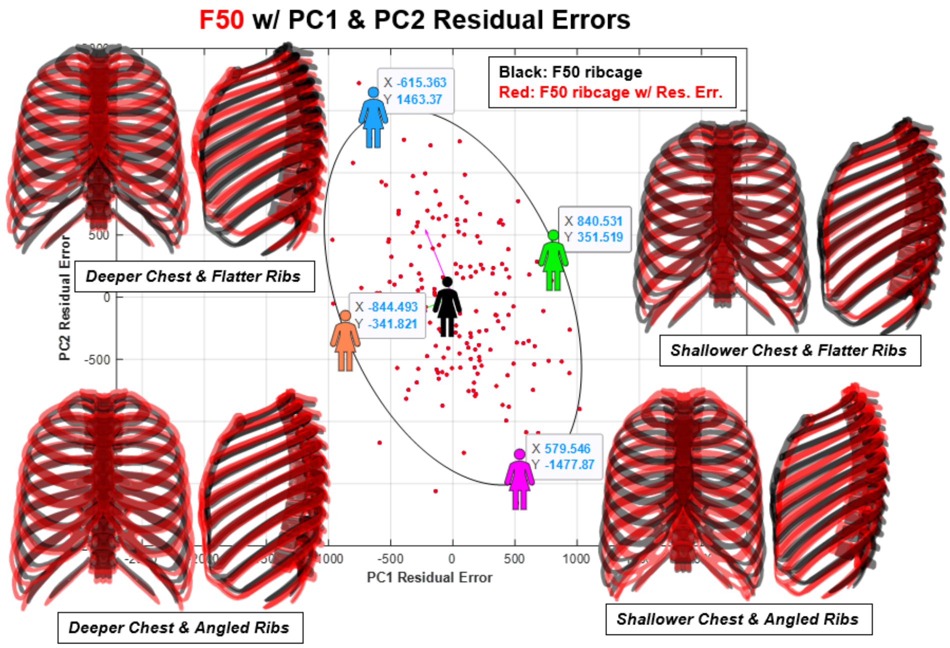

Figure 7. Varied ribcage geometries for midsize males (top) and midsize females (bottom)

Pelvis Geometry Residual Errors

Figure 8 shows the percentage of total variance explained by each PC (left) and the PC residual errors in male and female subjects (right) for the pelvis geometry model. The first two PCs accounted for over 52 percent of the total geometric variance in the pelvis. The residual errors are also distributed wider in the first two PCs.

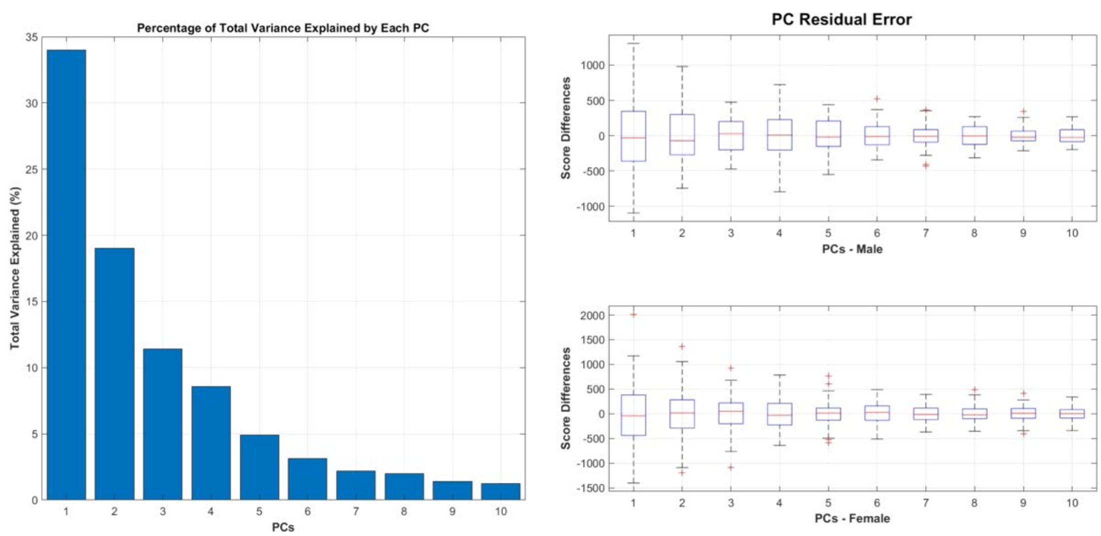

Figure 8. PCA and residual error results for the pelvis geometry model

Figure 9 shows the residual error distributions for the first five PCs of the pelvis with respect to subject stature and BMI. The residual errors do not have any strong correlations to the subject covariates, meaning that any specific subject shares the same residual error as the whole male or female population.

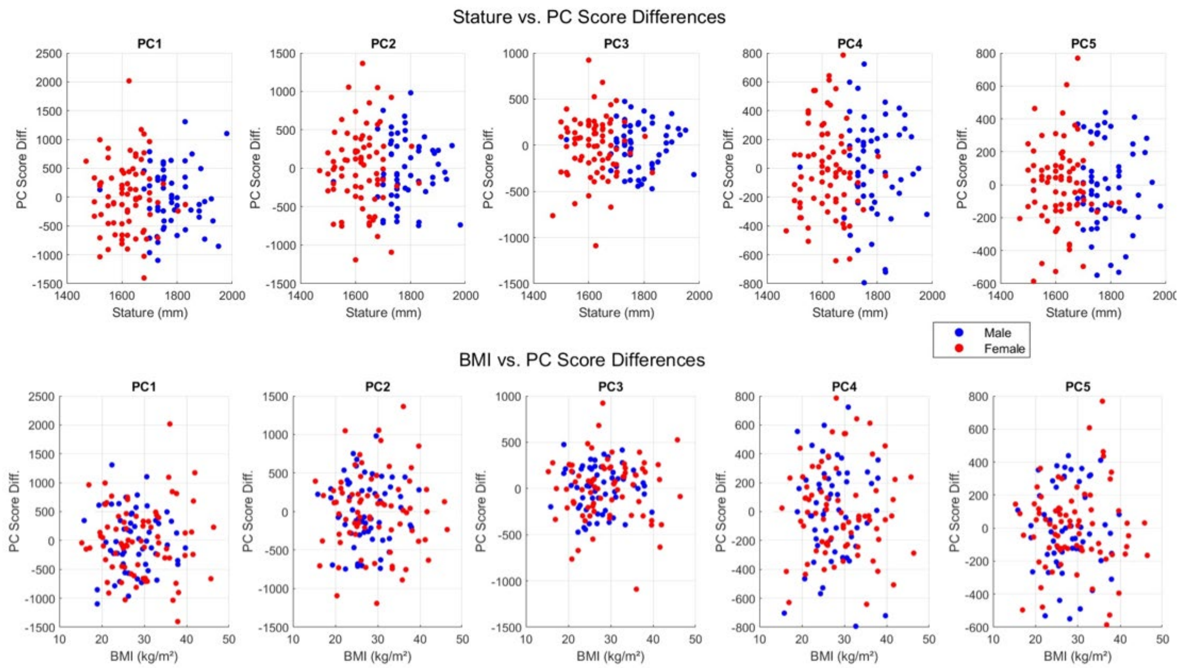

Figure 9. Residual error distributions in the first five PCs of pelvis

Figure 10 shows the residual error effects on the midsize male pelvis. Overall, the residual errors of PC1 and PC2 have stronger effects on the pelvis geometry than other PCs. Specifically, PC1 affects the size of the pelvis, and PC2 affects the shape of pelvis, especially in the sacrum area.

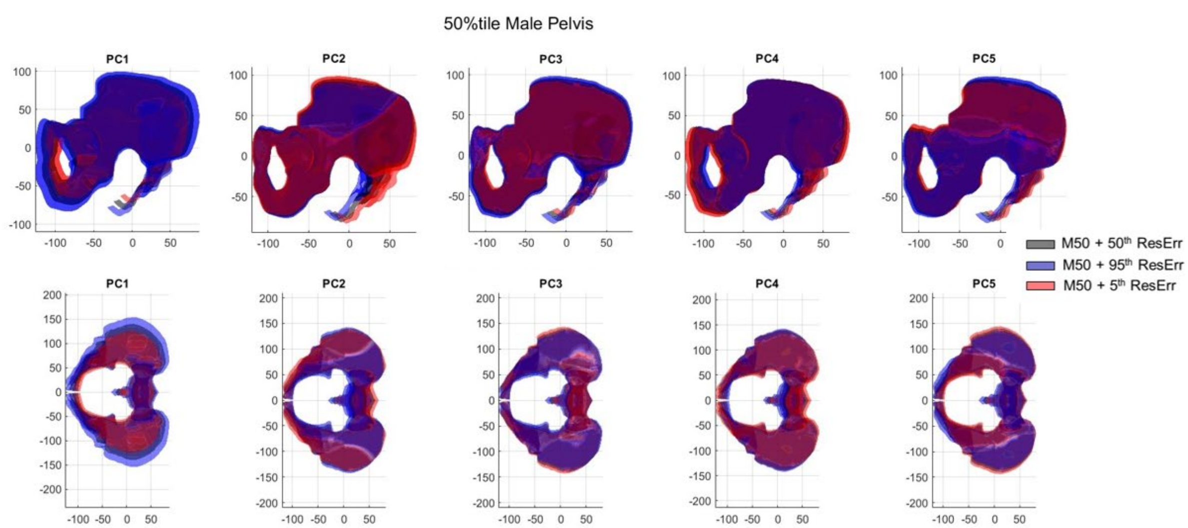

Figure 10. Residual error effects on the first five PCs for midsize male pelvis

Figure 11 shows five pelvis geometries for midsize males and five for midsize females. The black color represents the average midsize male or midsize female. The four blue pelvis and four red pelvis geometries are at the vertices/co-vertices of the major and minor axes of the ellipse that covers 95 percent of the residual errors for males and females. These pelvis models show clear size and shape variations in the midsize male and female populations.

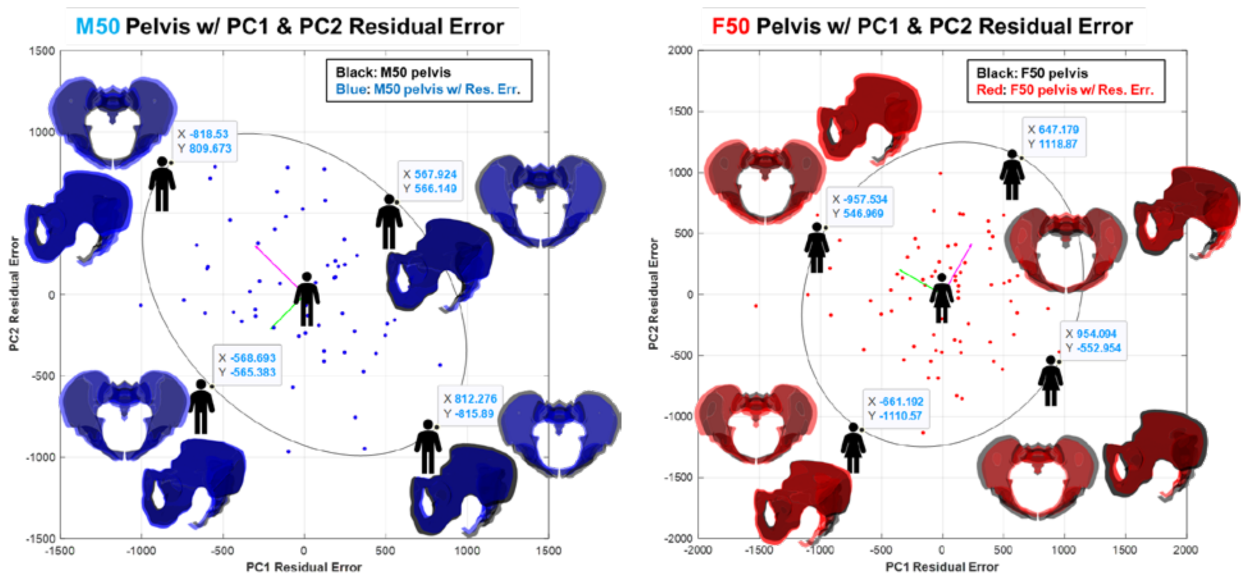

Figure 11. Varied pelvis geometries for midsize males (left) and midsize females (right)

Femur Geometry Residual Errors

Figure 12 shows the percentage of total variance explained by each PC (left) and the PC residual errors in all sampled subjects (right) for the femur geometry model. PC1 dominated the variance by accounting for over 80 percent of the total geometric variance in the femur. Opposite to ribcage and pelvis, the residual error in PC1 of the femur has lower variations than those from other top PCs.

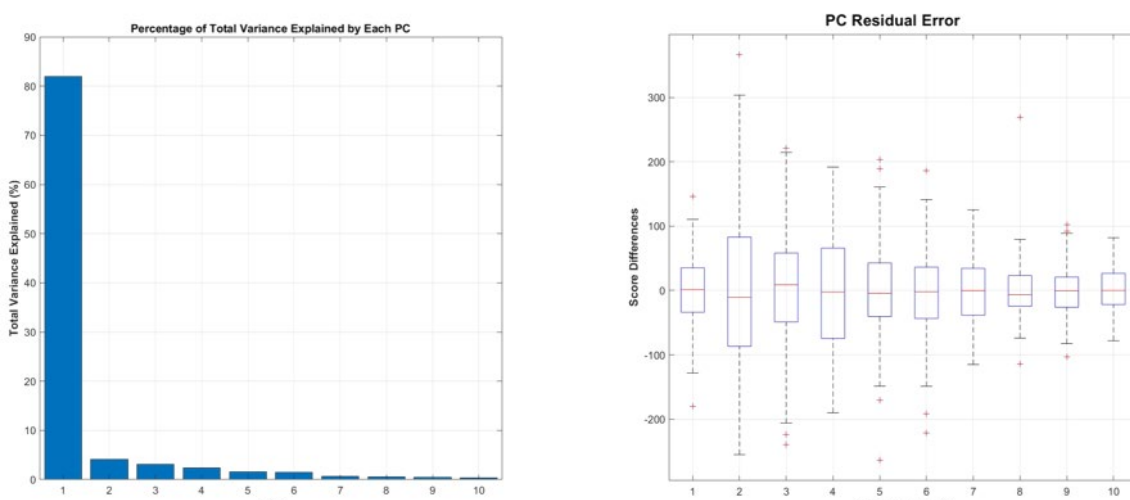

Figure 12. PCA and residual error results for the femur geometry model

Figure 13 shows the residual error distributions for the first PC of the femur with respect to femur length, BMI, and age. The residual errors do not have any strong correlations to the subject covariates, meaning that any specific subject shares the same residual error as the whole population.

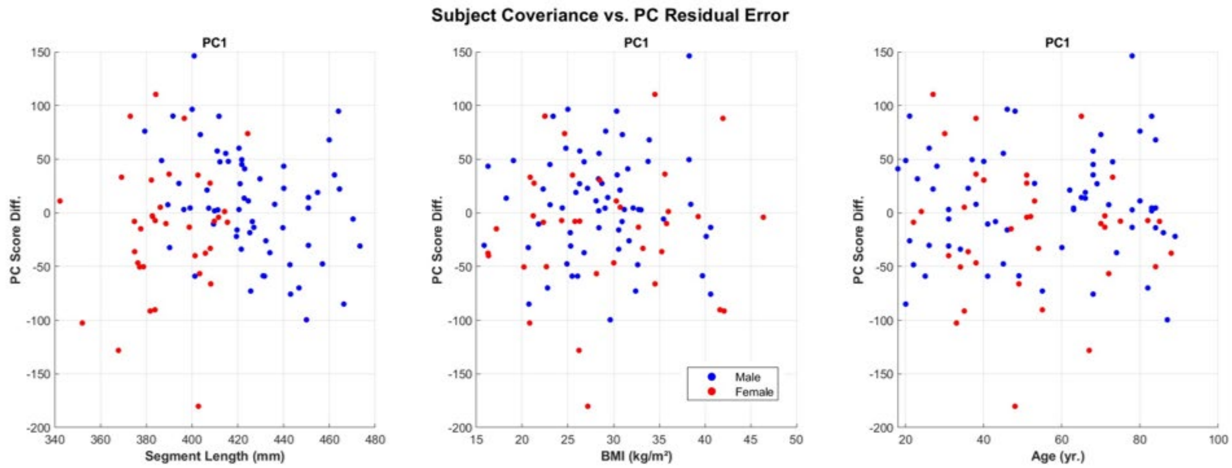

Figure 13. Residual error distributions in the first PC of femur

Figure 14 shows the residual error effects on the midsize male and midsize female femur. There is no significant effect from the residual error of any PC on the femur geometry, suggesting that the variability of the femur geometry in midsize males and midsize females is very much negligible.

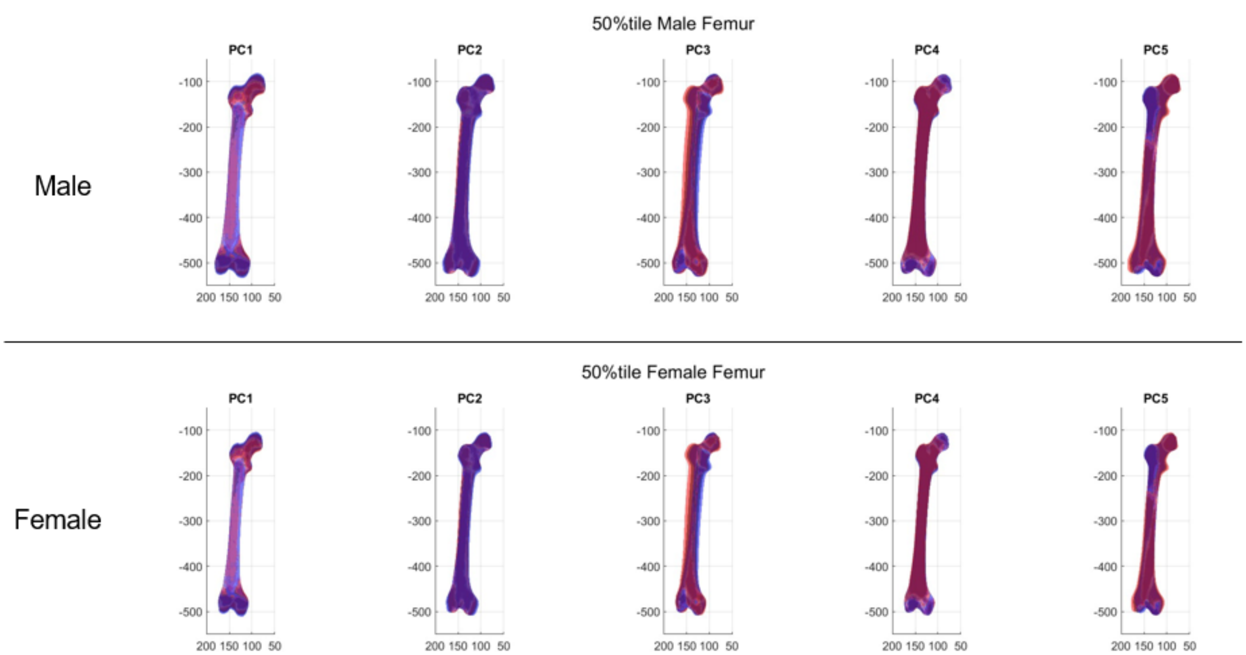

Figure 14. Residual error effects on the first five PCs for midsize male femur

Tibia Geometry Residual Errors

Figure 15 shows the percentage of total variance explained by each PC (left) and the PC residual errors in all sampled subjects (right) for the tibia geometry model. PC1 dominated the variance by accounting for over 82 percent of the total geometric variance in the tibia. Like the femur, the residual error in PC1 of the tibia has lower variations than those from other top PCs.

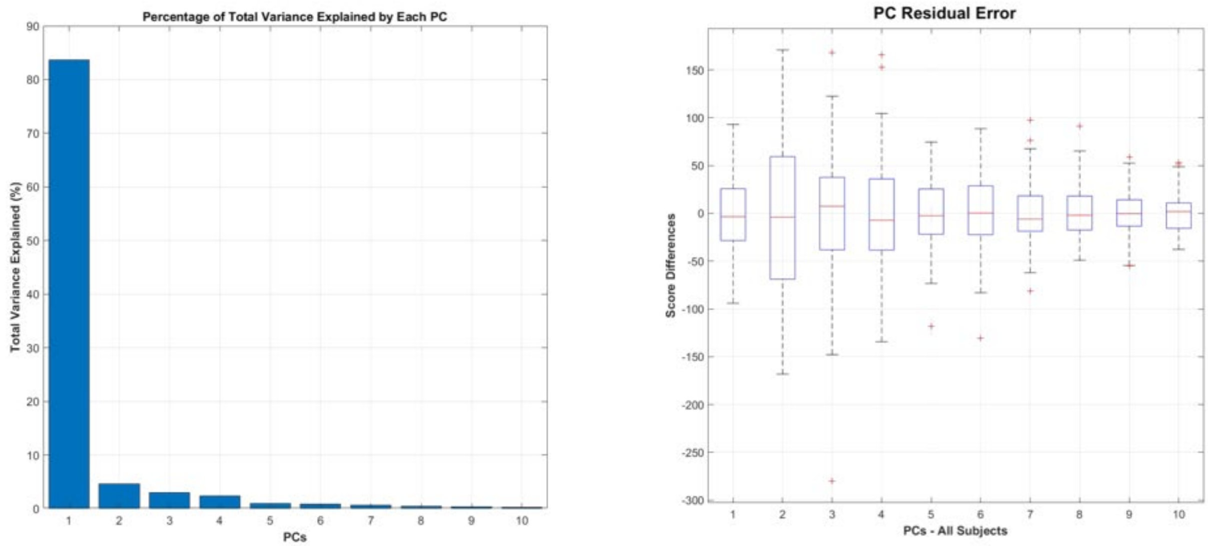

Figure 15. PCA and residual error results for the tibia geometry model

Figure 16 shows the residual error distributions for the first PC of the tibia with respect to tibia length, BMI, and age. The residual errors do not have any strong correlations to the subject covariates, meaning that any specific subject shares the same residual error as the whole population.

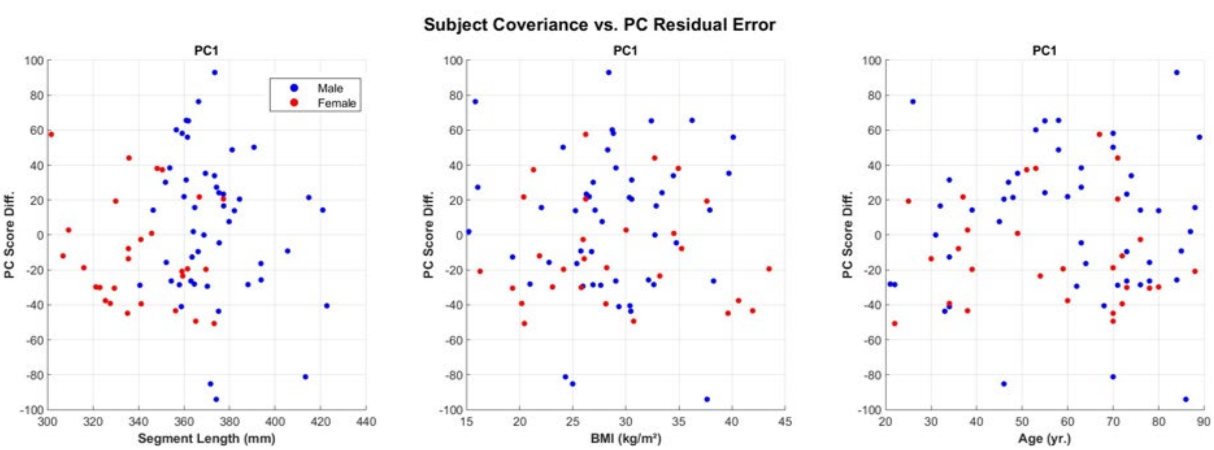

Figure 16. Residual error distributions in the first PC of tibia

Figure 17 shows the residual error effects on the midsize male and midsize female tibia. There is no significant effect from the residual error of any PC on the tibia geometry, suggesting that the variability of the tibia geometry for the midsize males and midsize females is negligible.

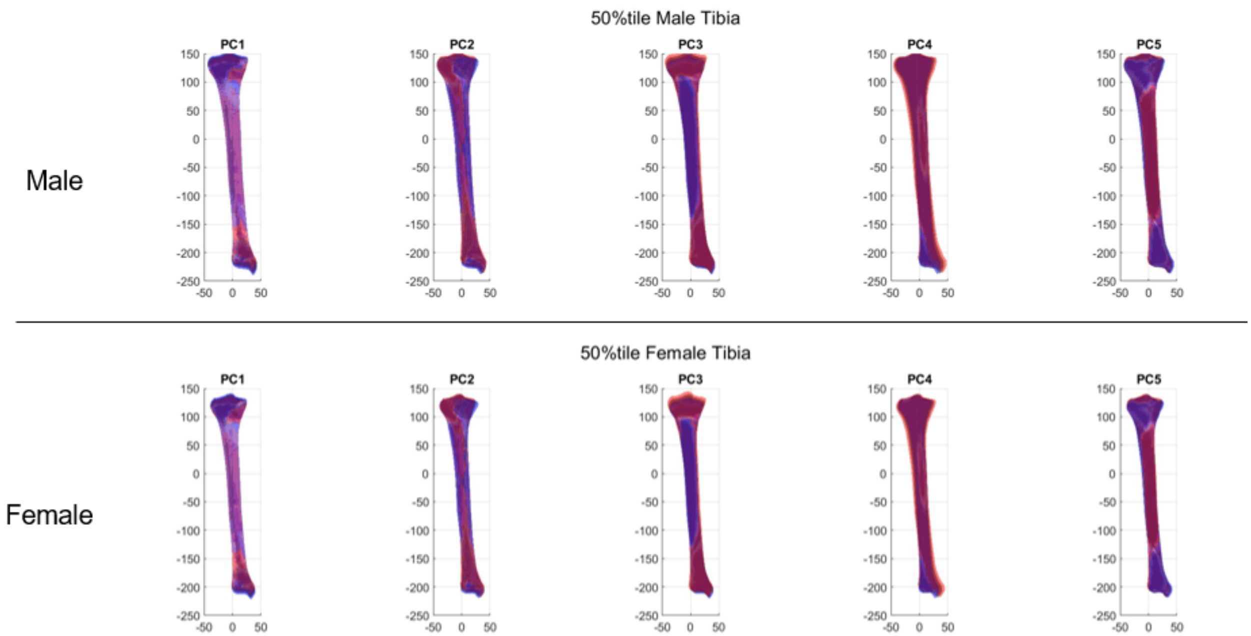

Figure 17. Residual error effects on the first five PCs for midsize male tibia

External Body Shape Residual Errors

Figure 18 shows the percentage of total variance explained by each PC (left) and the PC residual errors in male and female subjects (right) for the external body shape model. The first three PCs dominated the variance by accounting for over 77 percent of the total geometric variance in the external body shape. The residual errors are also distributed wider in the first three PCs than the rest of the PCs.

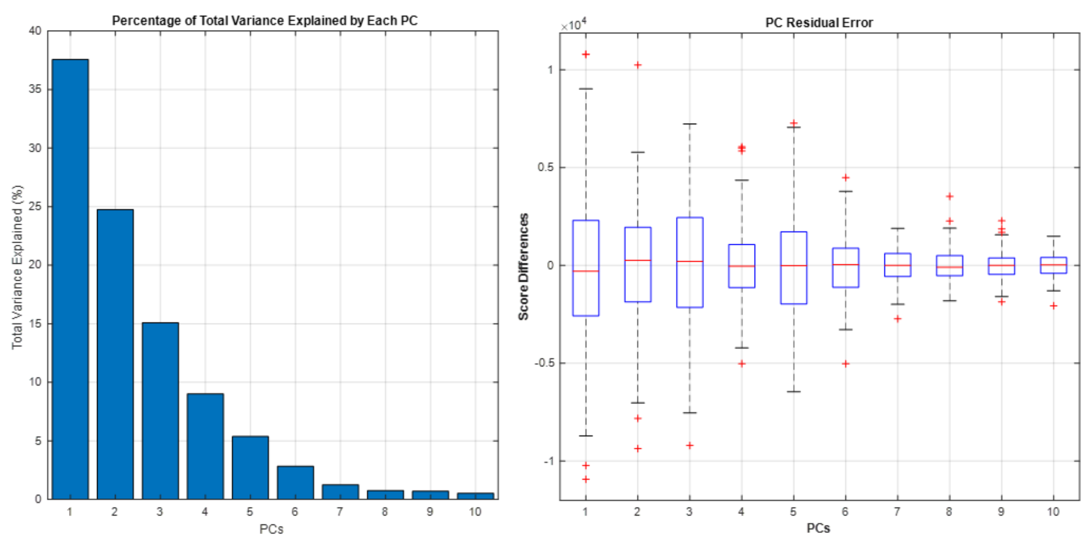

Figure 18. PCA and residual error results for the external body shape model

Figure 19 shows the residual error effects on the midsize male external body shape. Overall, the residual errors of three PCs have stronger effects on the external body shape than the other PCs. However, the PC1 and PC3 are more related to the body position/posture, while PC2 is related to the sitting height, which is less relevant to the shape of the body surface. PC 7 and PC 8 are more related to the body shape, but they account for relatively low variance in the midsize male.

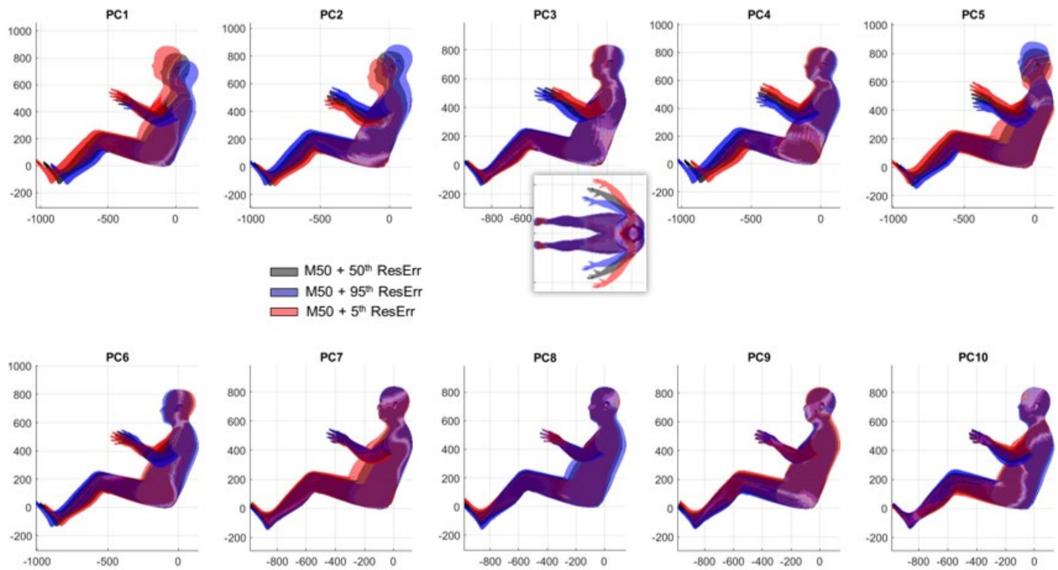

Figure 19. Residual error effects on the first ten PCs for midsize male external body shape

Figure 20 shows five external body shapes for midsize males and five for midsize females. The black color represents the average midsize male or midsize female. The four blue external body shapes and four red external body shapes are at the vertices/co-vertices of the major and minor axes of the ellipse that covers 95 percent of the residual errors in PCs 7 and 8 for males and females. These external body shapes show clear torso shape variations in the midsize male and female populations.

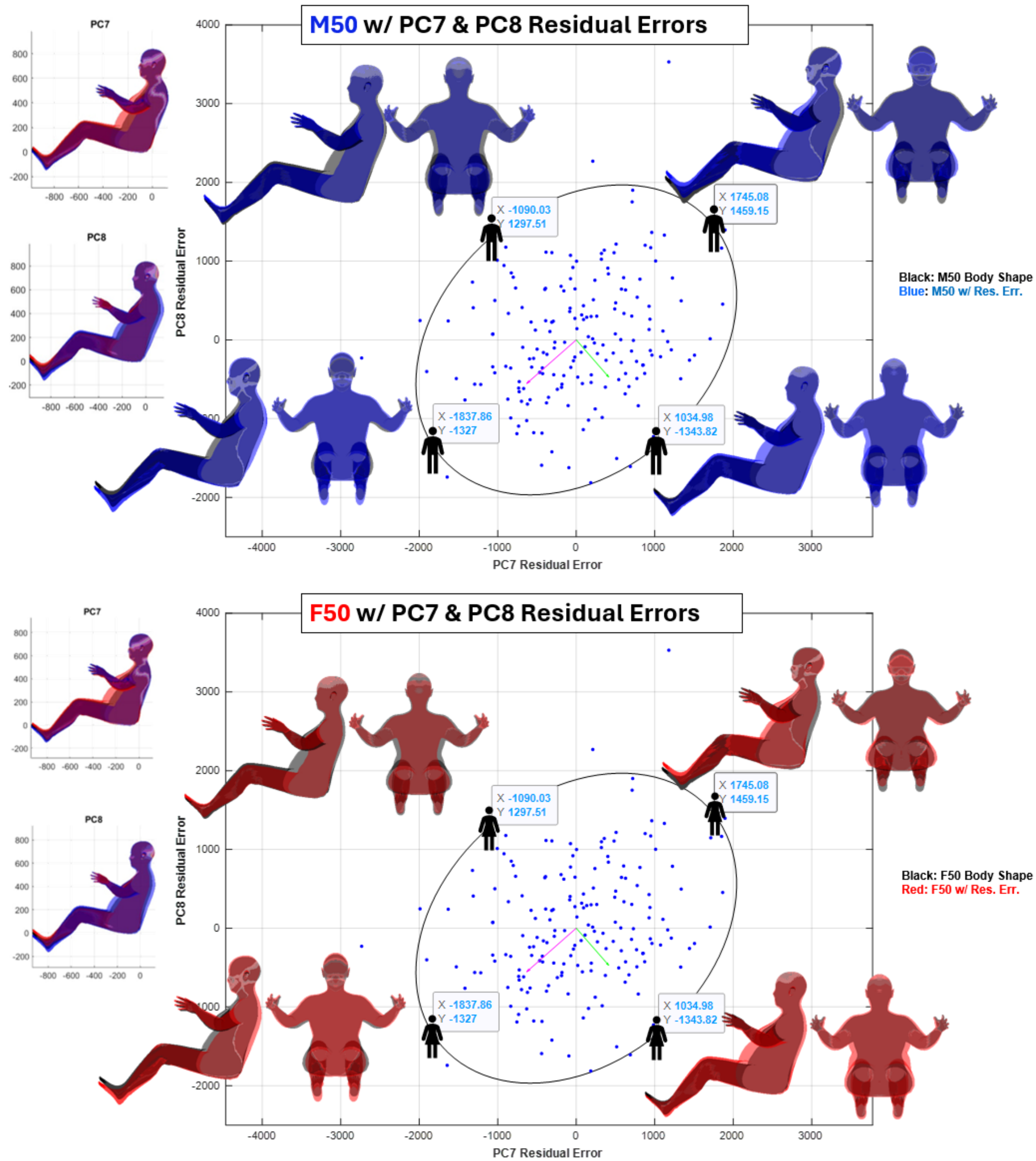

Figure 20. Varied external body shapes for midsize males (top) and midsize females (bottom)

This page is intentionally left blank.

Task 2: HBM Mesh Morphing

The goal of this task is to use the mesh morphing method to develop a set of male and female FE HBMs accounting for the geometric variations quantified in Task 1.

Combined Whole-Body Geometric Variations for Midsize Males and Midsize Females

As described in the previous sections, the residual errors in the ribcage and pelvis geometries in midsize males and midsize female are significant, while those in the femur and tibia are not significant. The residual errors in external body shape are quite complex, which are dominated by body position/posture. Based on these findings, we decided to consider only the ribcage and pelvis geometry variations in the whole-body geometry model and treat them as independent from each other. Therefore, the external body shape was only varied based on the ribcage and pelvis geometries. As a result, eight midsize female models were generated, including four with varied ribcage and four with varied pelvis geometries, as shown in Figure 21. Similarly, eight midsize male models were generated, including four with varied ribcage and four with varied pelvis geometries, as shown in Figure 22. It should be noted that the ribcage and pelvis geometric variations affected the torso length, and as a result affected the sitting height of the models. The external body surface was fine-tuned based on the skeleton geometries to ensure good fit.

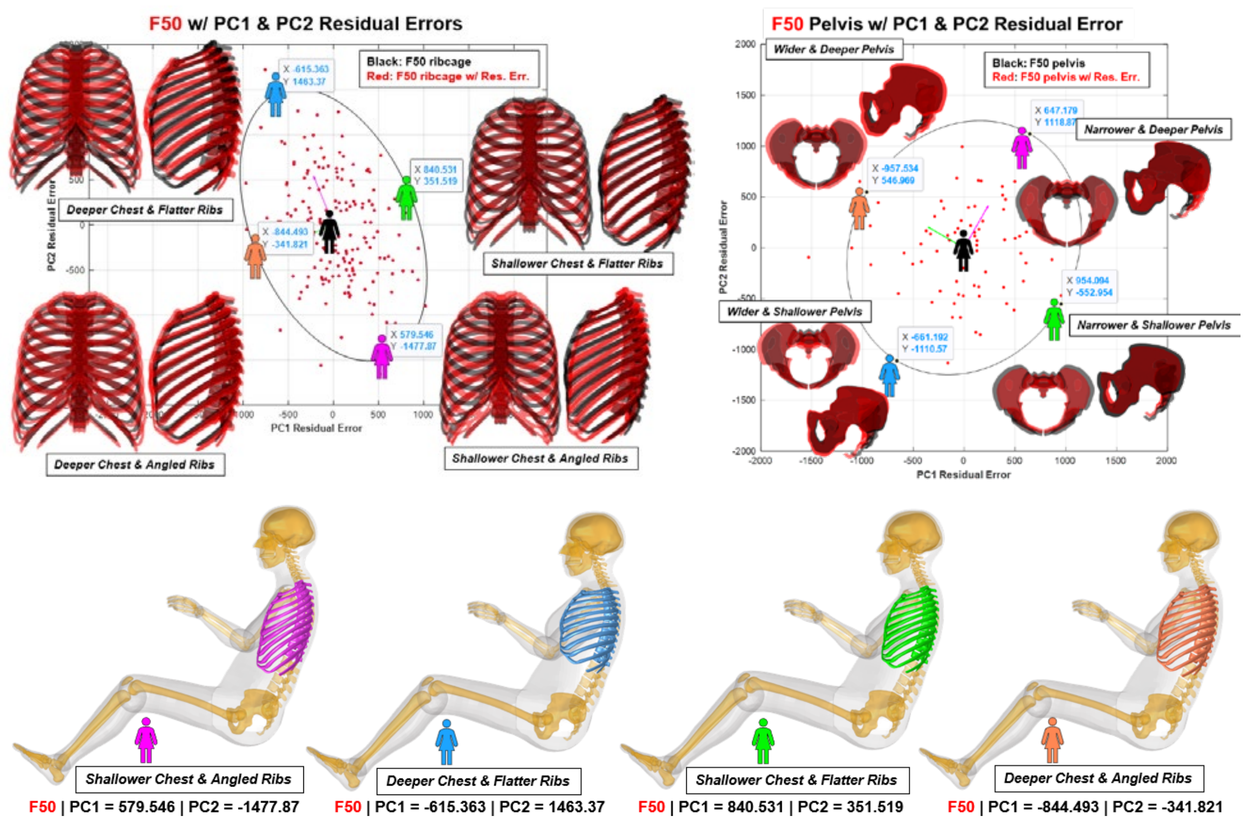

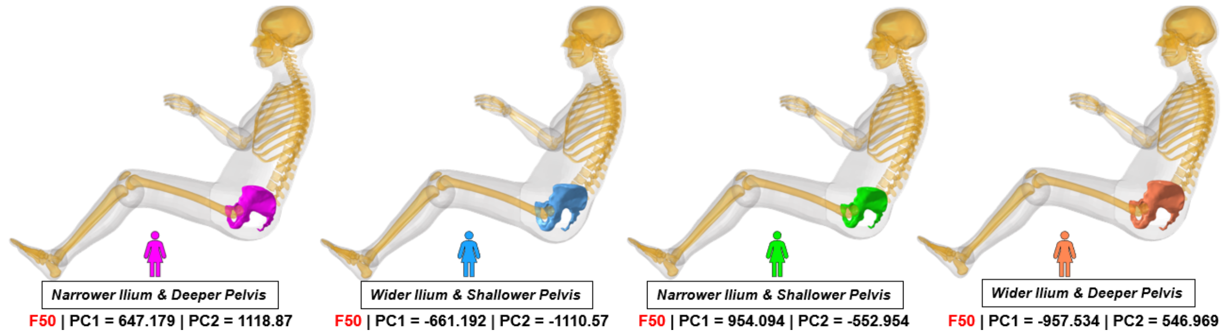

Figure 21. Representative midsize female geometries with ribcage and pelvis variations

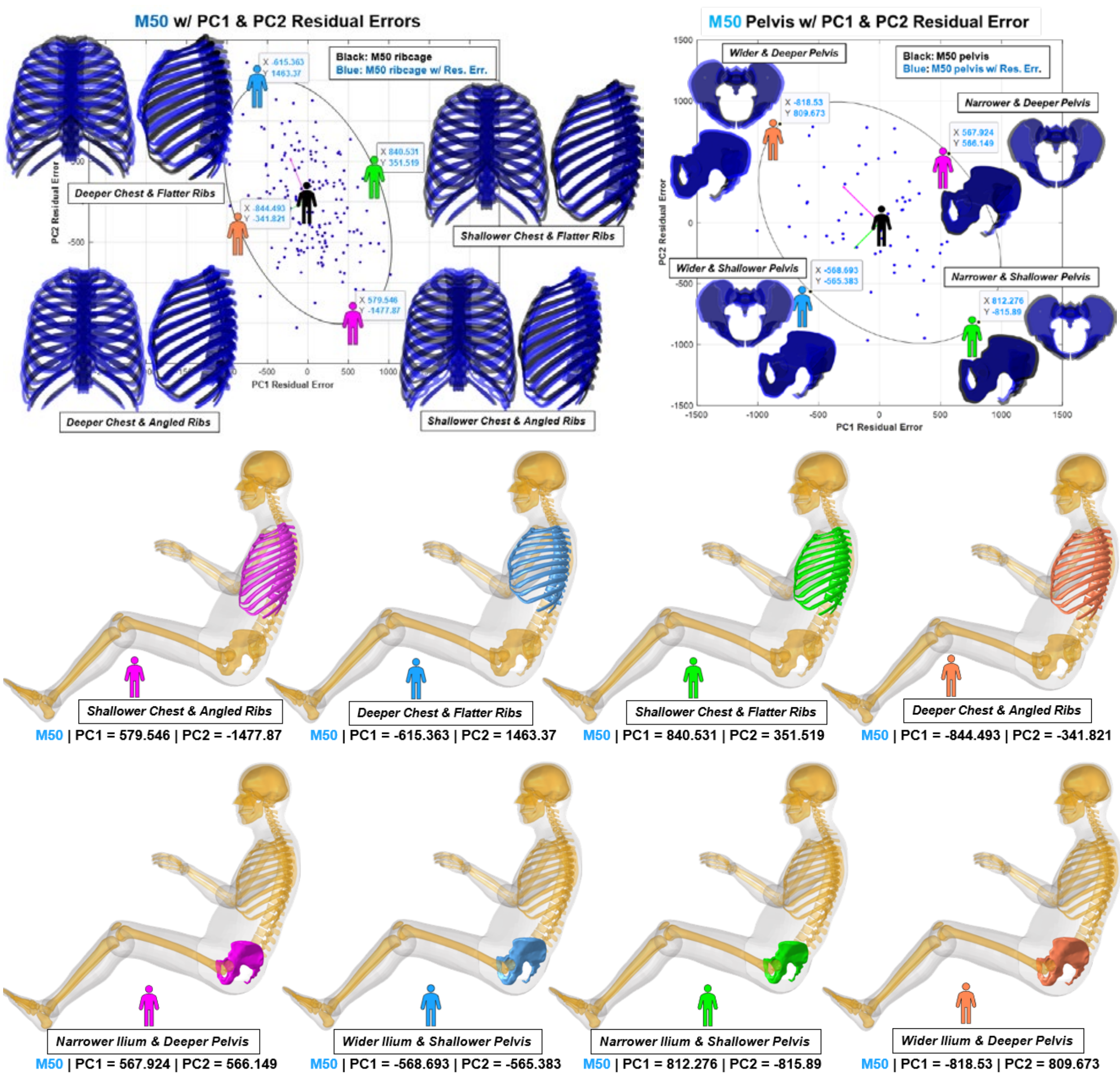

Figure 22. Representative midsize male geometries with ribcage and pelvis variations

Mesh Morphing Process

Our previous work has resulted in a comprehensive mesh morphing framework to morph a baseline FE HBM model into the predicted target geometry by the statistical geometry model. The primary landmark-based mesh morphing algorithm based on radial basis functions has been well documented in our previous publications (Hu, 2018; Hu et al., 2019b; Hwang et al., 2019; Tang et al., 2020; Zhang et al., 2017). To morph baseline models (i.e., THUMS and GHBMC) into geometries predicted by the same set of statistical skeleton and body shape models, each of the baseline models must be linked to the statistical geometry models. To do that, each baseline model is treated as a subject in the same way as that used for collecting the geometry data. Specifically, landmarks are first identified on each of the 24 ribs, sternum, pelvis, femurs, tibias, and other bones, along with the external body shape on the baseline models. Then the template meshes used to develop statistical geometry models are morphed and projected onto the corresponding skeleton and body shape surface meshes of the baseline models. This mesh mapping process sets up the correspondence between the template meshes of the statistical geometry models and the surface meshes from the baseline models. After that, with any given age, sex, stature, SHS, and BMI, the surface meshes of the skeleton and the external body shape in the baseline model are automatically morphed into the statistical-model-predicted geometry. These morphed surface-meshes serve as the landmarks for morphing all the other components in the whole body.

The mesh morphing sequence is shown in Figure 23, in which the GHBMC M50-OS model is morphed into a midsize female geometry from our statistical models.

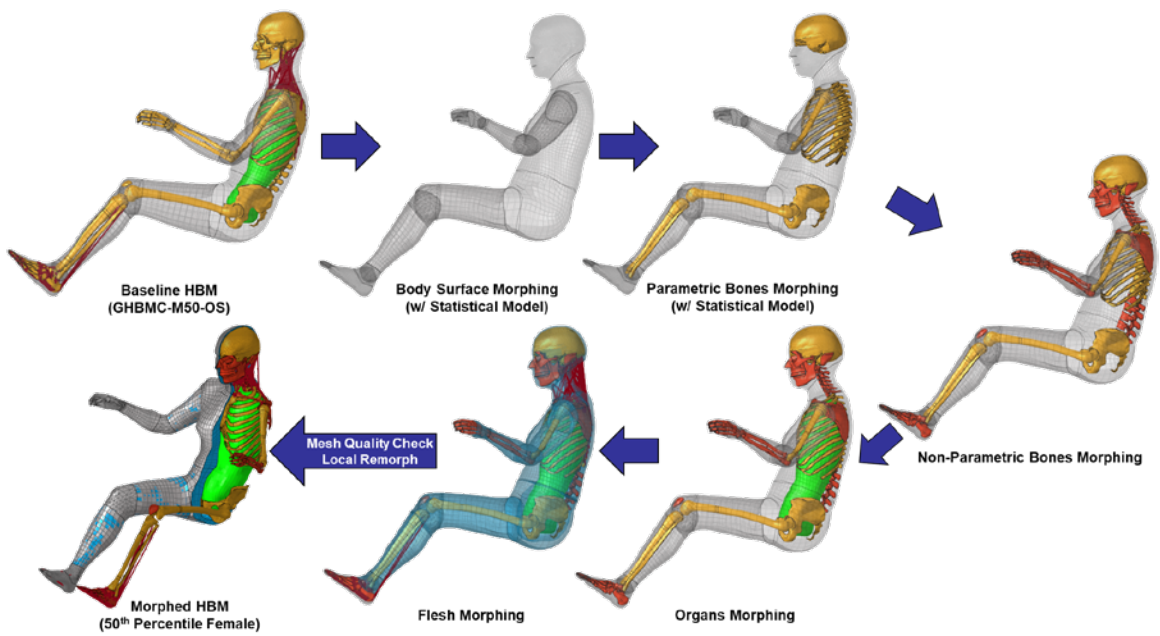

Figure 23. Illustration of morphing sequence

The following steps were used in the process shown in Figure 23:

1) **Statistical skeleton and body surface** – Skeleton and external body surface models were morphed to the geometry as described in Task 1.
2) **Other skeleton models** – Bones without statistical geometry models were morphed by surrounding bones and bony landmarks in the external body surface model.
3) **Connective tissues** – Connective tissues, such as ligaments and intervertebral discs, were morphed based on the bone geometries.
4) **Head and brain** – Soft tissues in the head, including flesh and brain, were morphed based on skull and scalp/face surface.
5) **Flesh and organ boundary** – A layer representing the abdominal wall was identified and morphed by the ribcage, pelvis, and spine.
6) **Flesh** – All flesh in the torso and extremities were morphed component-by-component following the sequence of pelvis, lower extremities, lower torso, upper torso, upper extremities, and neck.
7) **Internal organs** – Internal organs were morphed together based on the skeleton geometries.
8) **Mesh quality check and re-morph** – Sometimes, a single mesh morphing cannot achieve satisfactory mesh quality. For these cases, mesh morphing was used regionally to smooth the mesh and fix bad elements. We refer this method as a local "re-morph." While mesh qualities in bones are generally good, all other parts can be re-morphed by their neighboring nodes to improve the mesh quality. A re-morphing function requires using Hypermesh to check the mesh quality before and after re-morph, and an automatic local re-morph for bad elements.

Morphed HBMs

A total of 18 morphed models, including nine for 50th percentile males and nine for 50th percentile females, were developed by morphing the GHBMC M50-OS v2.3 model. All morphed HBMs are with reasonable mesh quality as shown in Table 3.

Table 3. Mesh quality for all morphed models

HBM	Variation	Description	2D JCB < 0.3	2D JCB < 0.3 (%)	Min. 2D JCB	3D JCB < 0.3	3D JCB < 0.3 (%)	Min. 3D JCB
F50	Pelvis	Wider & Shallower Pelvis	8	0.00004	0.03	83	0.00062	0.15
F50	Pelvis	Wider & Deeper Pelvis	8	0.00004	0.03	89	0.00066	0.16
F50*	**Pelvis**	**Midsize Pelvis**	8	0.00004	0.03	79	0.00059	0.17
F50	Pelvis	Narrower & Deeper Pelvis	9	0.00004	0.03	84	0.00062	0.16
F50	Pelvis	Narrower & Shallower Pelvis	8	0.00004	0.03	83	0.00062	0.16
F50	Ribcage	Deeper Chest & Flatter Ribs	7	0.00003	0.09	84	0.00062	0.15
F50	Ribcage	Deeper Chest & Angled Ribs	6	0.00003	0.18	82	0.00061	0.14
F50*	**Ribcage**	**Midsize Ribcage**	8	0.00004	0.03	79	0.00059	0.17
F50	Ribcage	Shallower Chest & Angled Ribs	10	0.00005	0.11	93	0.00069	0.16
F50	Ribcage	Shallower Chest & Flatter Ribs	8	0.00004	0.05	80	0.00059	0.17
M50	Pelvis	Wider & Shallower Pelvis	5	0.00002	0.06	107	0.00080	0.14
M50	Pelvis	Wider & Deeper Pelvis	6	0.00003	0.06	109	0.00081	0.14

HBM	Variation	Description	2D JCB < 0.3	2D JCB < 0.3 (%)	Min. 2D JCB	3D JCB < 0.3	3D JCB < 0.3 (%)	Min. 3D JCB
M50*	**Pelvis**	**Midsize Pelvis**	5	0.00002	0.06	102	0.00076	0.14
M50	Pelvis	Narrower & Deeper Pelvis	6	0.00003	0.06	103	0.00077	0.14
M50	Pelvis	Narrower & Shallower Pelvis	5	0.00002	0.06	103	0.00077	0.14
M50	Ribcage	Deeper Chest & Flatter Ribs	5	0.00002	0.11	112	0.00083	0.05
M50	Ribcage	Deeper Chest & Angled Ribs	5	0.00002	0.04	124	0.00092	0.02
M50*	**Ribcage**	**Midsize Ribcage**	5	0.00002	0.06	102	0.00076	0.14
M50	Ribcage	Shallower Chest & Angled Ribs	6	0.00003	0.19	118	0.00088	0.13
M50	Ribcage	Shallower Chest & Flatter Ribs	5	0.00002	0.08	106	0.00079	0.14
M50	**Baseline**	**GHBMC M50-OS v2.3**	**0**	**0.00000**	**0.35**	**2**	**0.00001**	**0.28**

*The F50 models with the midsize pelvis and midsized ribcage are the same model with average midsize female geometry, and the M50 models with the midsize pelvis and midsized ribcage are the same model as well. Each of them was presented twice in the table as the baseline model for better comparison.

This page is intentionally left blank.

Task 3: HBM Simulations

The goal of this task is to conduct impact simulations using the morphed HBMs for 50th percentile males and females in various impact conditions to evaluate the effects from geometry variations on occupant impact responses and injury outcomes.

Simulation Conditions and Matrix

The simulation conditions, reported outcomes, and associated references are shown in Table 4. Nine impact conditions were used for each of the morphed models, which resulted in 81 simulations for the 50th percentile female models and 81 simulations for the 50th percentile male models. The first seven impact conditions in Table 4 are well established post-mortem human subject (PMHS) testing conditions used for GHBMC model validations. We specifically added the last two U.S.-New Car Assessment Program (US-NCAP) frontal crash simulations because we recognize the morphed HBMs may be important for vehicle virtual testing in the future. Therefore, evaluating their response variations in US-NCAP testing conditions will be valuable.

Table 4. Simulation conditions

Boundary Condition	Outcome	Reference
Thorax hub impact (6.7 m/s)	F vs. D	(Lebarbé and Petit, 2012; Neathery, 1974)
Oblique abdomen/thorax hub impact (6.7 m/s)	F vs. t, F vs. D	(Viano, 1989)
Abdominal bar impact (6.0 m/s)	F vs. D	(Hardy et al., 2001)
Lateral shoulder impact (4.5 m/s)	F vs. t, D vs. t	(Koh et al., 2005)
Lateral pelvis impact (10.0 m/s)	F vs. D	(Bouquet et al., 1998)
Lateral sled impact (6.7 m/s)	F vs. t	(Cavanaugh et al., 1990)
Rear seat impact (13.3 m/s)	k, F vs. t	(Forman et al., 2009)
US NCAP frontal crash - Driver	Kinematics and injury measures	RAV4 (Figure 24)
US NCAP frontal crash - Passenger		

In this study, a validated driver and frontal passenger compartment model representing Toyota RAV4 was used for all US NCAP frontal crash simulations. The RAV4 model was developed and validated by Boyle et al. (2024). The model was based on a generic vehicle buck model developed by Iraeus and Lindquist (2016) which includes vehicle interior, driver airbag, crushable steering column, and driver seat. This generic model was further upgraded to include the front passenger interior and associated restraint system. The passenger instrument panel (IP) geometry was adjusted based on point stream data collected previously from 91 vehicles (Hu et al., 2014). After generating the passenger side geometry, a generic passenger IP airbag model, a generic scaled curtain airbag model, and a knee airbag model originally developed by ZF (Hu et al., 2019a) with recent updates were incorporated. The updated model was morphed to the scanned RAV4 interior geometry and further validated against RAV4 crash test data under US-NCAP frontal crash (35 mph) conditions by tuning the seat belt and airbag parameters. The process of mesh morphing and model validation are shown in Figure 24. Detailed results of model validation can be found in Boyle et al. (2024).

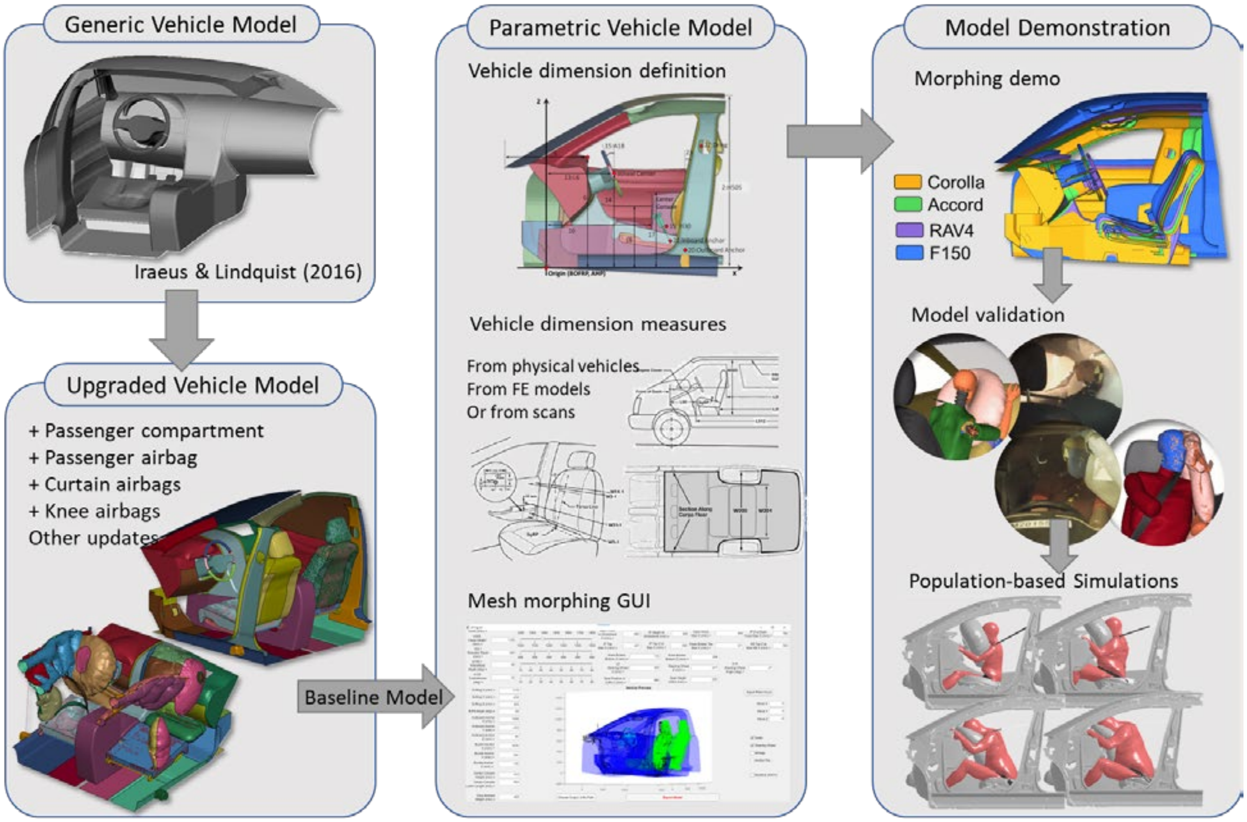

Figure 24. Method for developing the parametric vehicle model (Boyle et al., 2024)

Automated Simulation Setup and Data Collection

Crash conditions without a seat belt are typically easy to set up in an automated manner. We used MATLAB and Ls-Prepost CFILE templates to automate the process, including HBM and impactor positioning and model settling. We also established a robust method to integrate the occupant, restraint, and vehicle models together for vehicle crash simulations according to our previous work (Hu et al., 2019b). Specifically, we used a statistical seating posture model based on volunteer seating posture data to predict the head and hip locations with a given set of occupant characteristics and vehicle packaging parameters. The re-positioning tool calculates the joint angles associated with each joint and each of the morphed models was morphed into the target posture. Ls-Prepost was used to position the limbs with the existing tree structures defined in the human models, and a belt-fitting tool in MATLAB was used to automatically fit the seat belt on the occupant model based on the belt fit model from volunteer data. In the study, because the morphed HBMs with the same height have different sitting heights, the driver seat location and driving posture were slightly different between morphed HBMs even with the same weight and height. On the other hand, for the passenger side, we set the passenger seat at the same mid-rear location for all morphed HBMs, which left the same space for all occupants. These setup conditions differentiated the driver and passenger responses. Similar to the simulation setup, we used a combination of MATLAB code and Ls-Prepost CFILE templates to automate the data collection process.

For US-NCAP crash simulations, injury measures and injury probabilities to the head, chest, and lower extremities, were automatically collected. Scaling was used for the chest, femur, and tibia injury risk curves based on the sizes of the bony structures in the corresponding body regions. Age effect was not considered for predicting the chest injury risk, and all HBMs were set at 45 years old. All the injury risk curves and scaling methods used in this study are shown in Figure 25. The chest deflection was normalized by the chest depth, which is measured between the spinal process of T8 vertebra to the mid-sternum at the 4th intercostal space. The femur and tibia forces were normalized based on the cross-sectional area of the femur/tibia where load cells were defined for measuring the forces. The combined injury probability (Pjoint) was also calculated for all morphed models. It should be noted that neck injury risk was not considered in this study, because the neck injury risks are almost always near zero based on the HBM prediction.

Body Region	Injury Risk Curve	Scaling and reference
Head (HIC15) **Brain (BrIC)**	$\begin{cases} P_{HIC}(AIS3+) = \emptyset\left(\frac{ln(HIC15) - 7.45231}{0.73998}\right) \\ \text{where } \emptyset = \text{cumulative normal distribution} \\ P_{BrIC}(AIS3+) = 1 - e^{-(\frac{BrIC}{0.987})^{2.84}} \end{cases}$	Same injury risk curves were used for all human models (NHTSA, 2008; Takhounts et al., 2013)
Neck **(Nij, T/C in kN)**	$\begin{cases} P_{Nij}(AIS3+) = \frac{1}{1+e^{3.227-1.969Nij}} \\ P_T(AIS3+) = \frac{1}{1+e^{10.9745-2.375T}} \\ P_C(AIS3+) = \frac{1}{1+e^{10.9745-2.375C}} \\ P_{neck} = Max(P_{Nij}, P_T, P_C) \end{cases}$ $F = F_{subject} \times \frac{a_{midsize} \times b_{midsize}}{a_{subject} \times b_{subject}}$	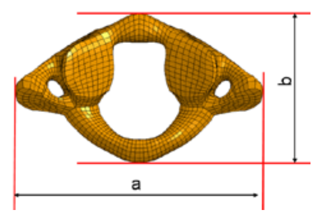 (NHTSA, 2008)
Chest **(D in mm)**	$P_{chest}(AIS3+) = \frac{1}{1+e^{10.5456-1.568*D^{0.4612}}}$ $P_{chest/Age}(AIS3+) = \frac{1}{1+e^{12.597-0.0586\text{Age}-1.568*D^{0.4612}}}$ $D = D_{subject} \times \frac{Depth_{midsize}}{Depth_{subject}}$	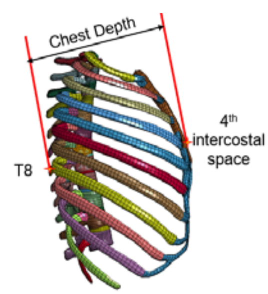 (Laituri et al., 2005)
Knee-Thigh-Hip **KTH** **And Tibia** **(F in kN)**	$P_{KTH}(AIS2+) = \frac{1}{1+e^{5.795-0.5196F}}$ $P_{TibiaU}(AIS2+) = \frac{1}{1+e^{5.7415-0.8189F}}$ $P_{TibiaL}(AIS2+) = \frac{1}{1+e^{3.7544-0.4683F}}$ $F = F_{subject} \times \frac{a_{midsize} \times b_{midsize}}{a_{subject} \times b_{subject}}$	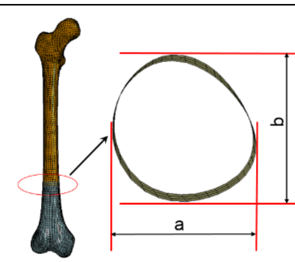 (Craig et al., 2020; NHTSA, 2008)
Whole Body	$P_{joint} = 1 - (1 - P_{head}) \times (1 - P_{chest}) \times (1 - P_{femur}) \times (1 - P_{tibiaU}) \times (1 - P_{tibiaL})$	

Figure 25. Injury risk curves and scaling method (Hu et al., 2019b)

Simulation Results

Component-Level Impact Responses

Figures 26 to 31 show the HBM impact responses from the component-level impact conditions described in Table 4, all conducted without a seat belt. Different numbers (*n*=5 or 9) of HBMs for F50 and M50 occupants were used in each impact condition. For instance, only five HBMs (1 midsize and 4 with ribcage variation) were used for both F50 and M50 occupants in the frontal thorax hub impact condition, as pelvis geometry variations are unlikely to affect the thoracic impact response in this scenario. In contrast, nine HBMs (1 midsize, 4 with ribcage variations, and 4 with pelvis variations) were used for both F50 and M50 occupants in the lateral sled impact condition, where both ribcage and pelvis geometry variations affect the impact response. The PMHS response corridors are shown in dashed lines in Figures 26 to 31. Note that all HBM responses for F50 are scaled to the M50 based on height and weight, so that they can be compared directly to the M50 PMHS corridors. Additionally, the curve colors in Figures 26 to 31 correspond to the HBM colors shown in Figures 21 and 22.

Based on the simulation results under component-level impact conditions, geometry variations in both F50 and M50 occupants influence impact responses to varying degrees across all scenarios. However, these variations are generally much smaller than the corresponding PMHS test corridors. The HBM impact responses showed the least variation in the abdominal bar, oblique abdomen/thorax hub, and lateral sled impact conditions, while greater variations were observed in the frontal thorax hub, lateral pelvis, and lateral shoulder impact conditions. It is intuitive that ribcage and pelvis geometries predominantly influence the responses in the frontal thorax hub and lateral pelvis impacts, respectively. However, it is noteworthy that ribcage geometry also affected the responses considerably in the lateral shoulder impact condition.

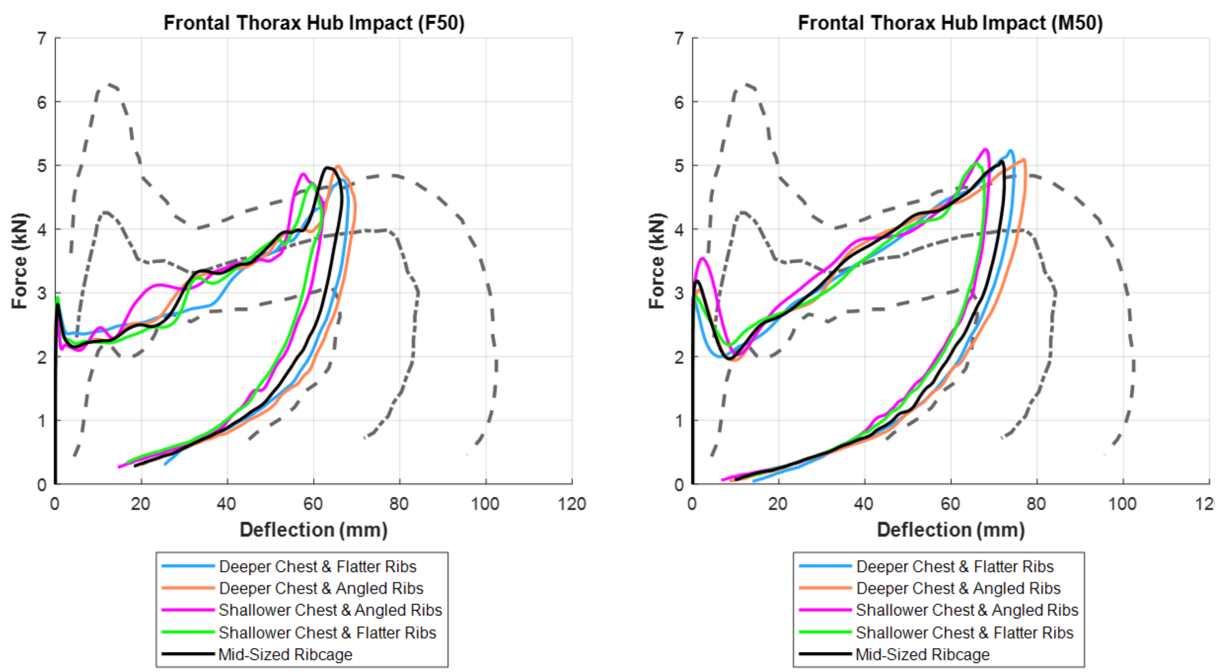

Figure 26. Frontal thorax hub impact responses for 50th percentile females (n=5 scaled) and 50th percentile males (n=5)

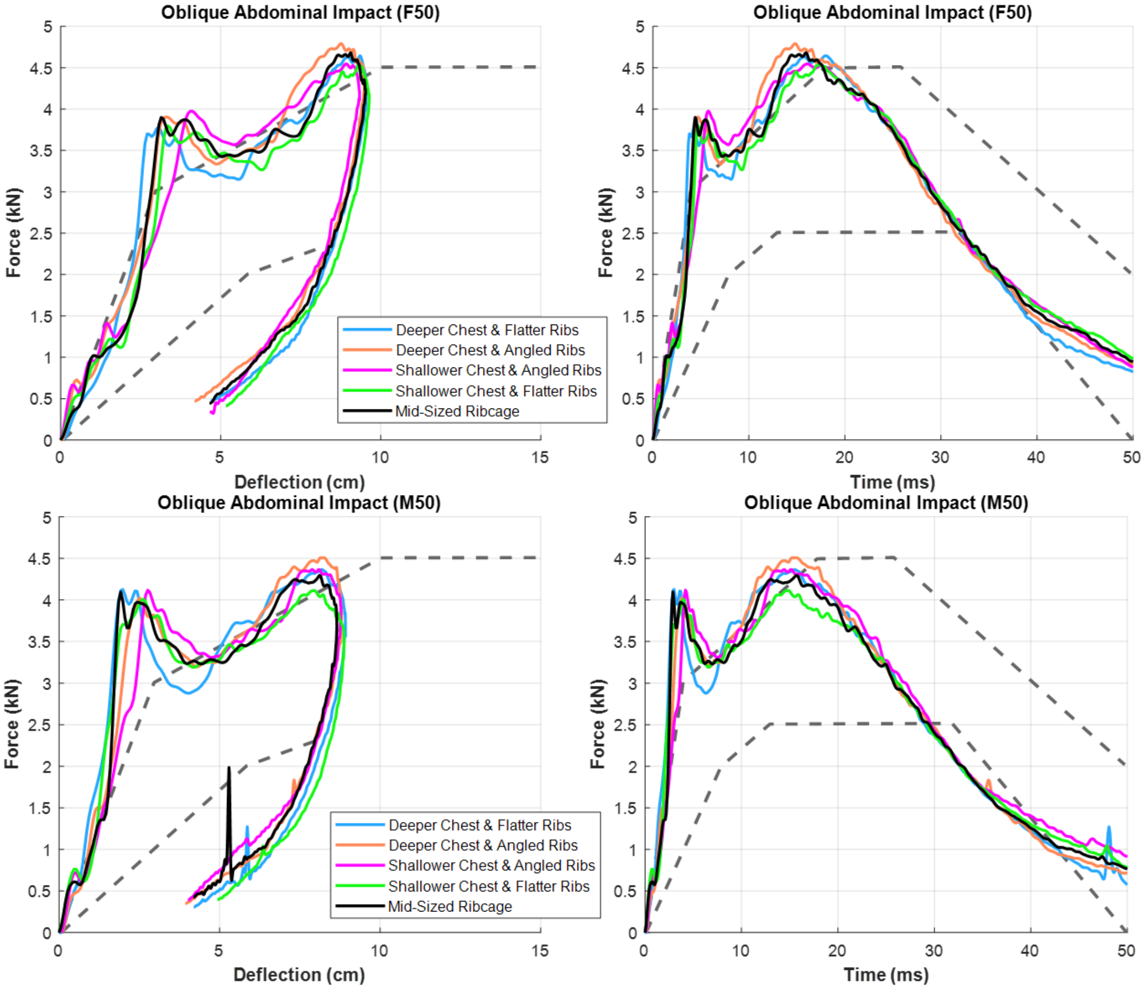

Figure 27. Oblique abdomen/thorax impact responses for 50th percentile females (n=5 scaled) and 50th percentile males (n=5)

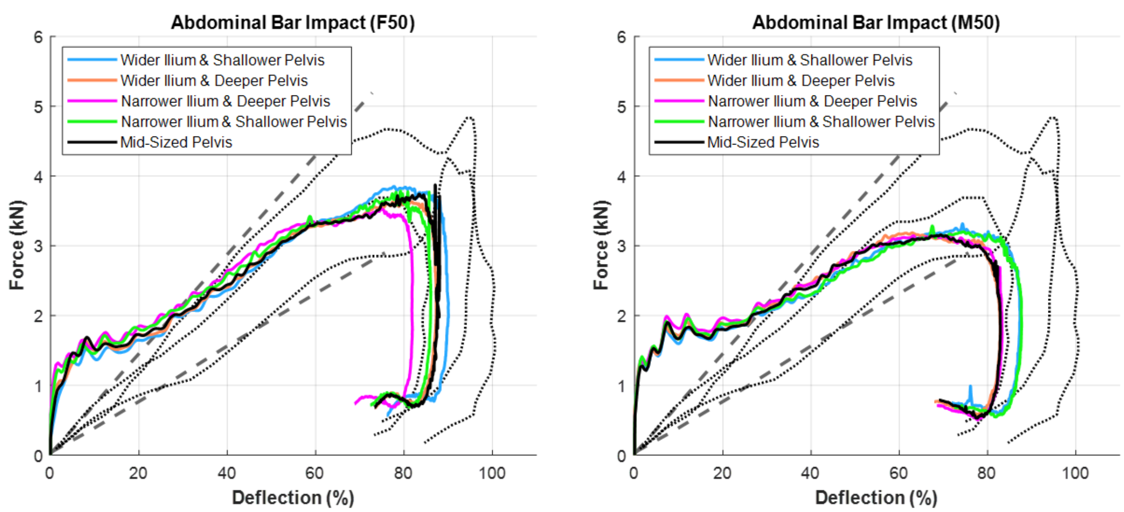

Figure 28. Abdominal bar impact responses for 50th percentile females (n=5 scaled) and 50th percentile males (n=5)

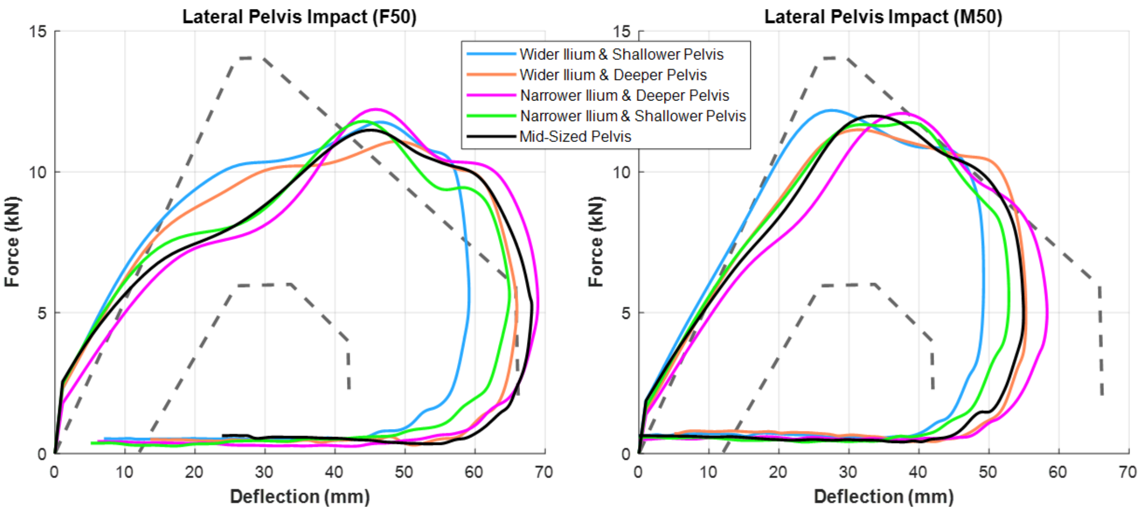

Figure 29. Lateral pelvis impact responses for 50th percentile females (n=5 scaled) and 50th percentile males (n=5)

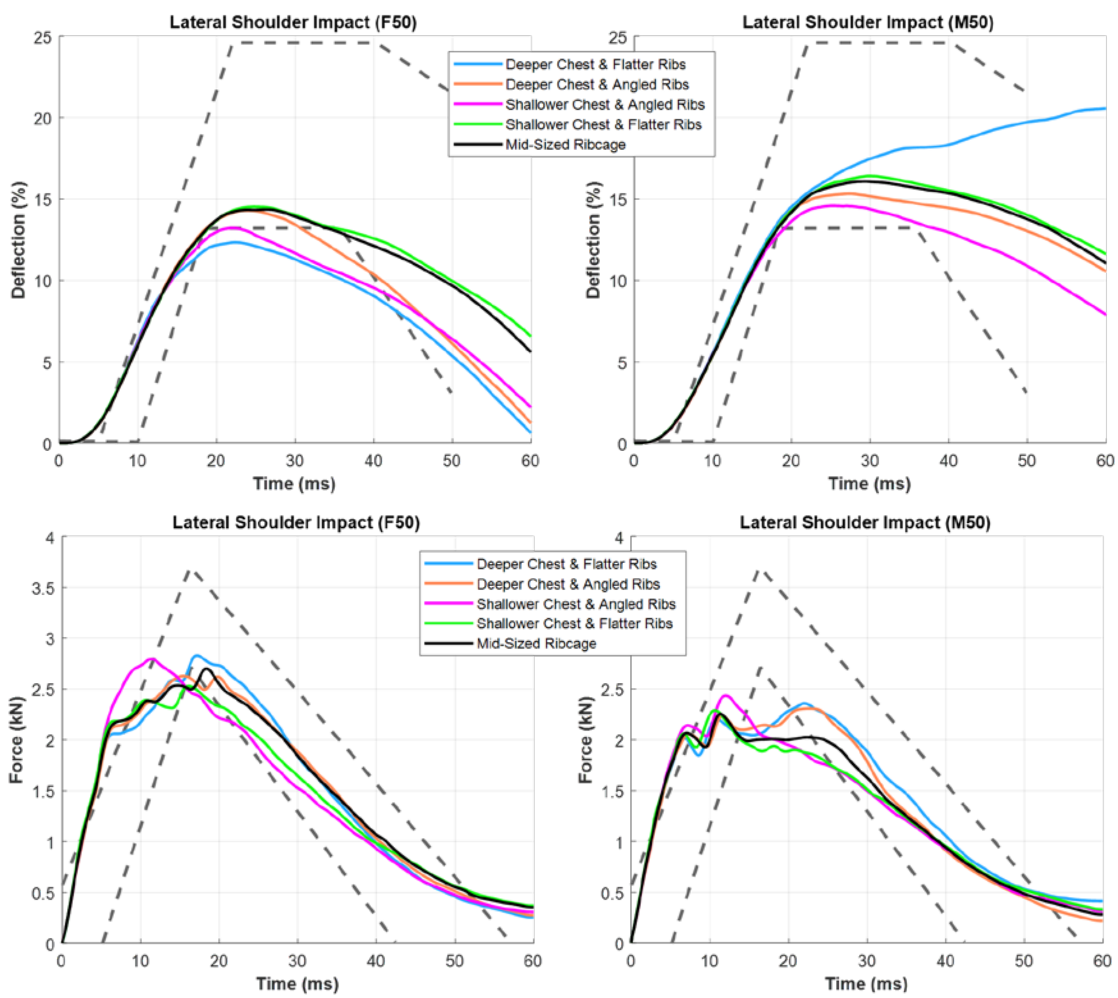

Figure 30. Lateral shoulder impact responses for 50th percentile females (n=5 scaled) and 50th percentile males (n=5)

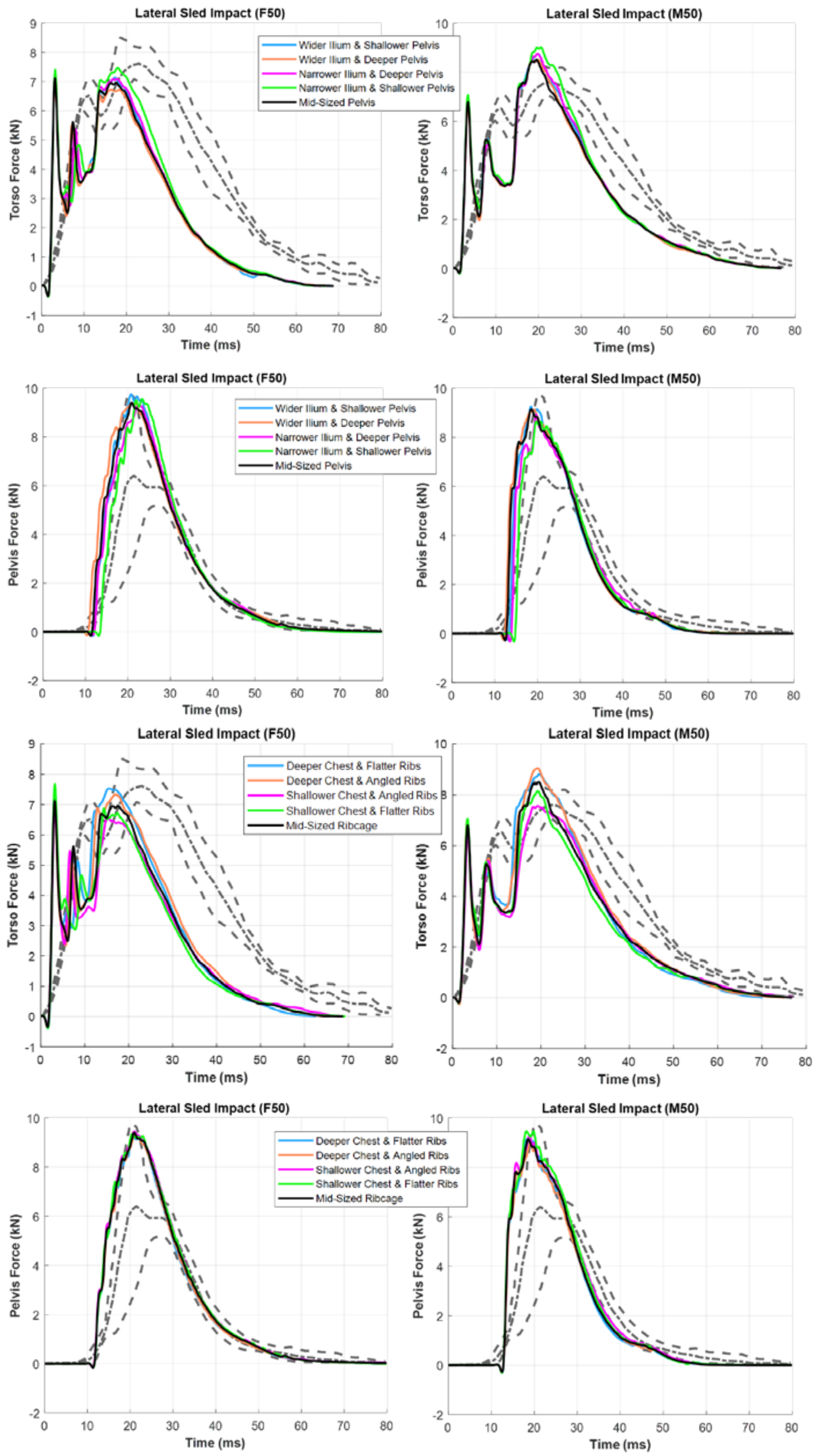

Figure 31. Lateral sled impact responses for 50th percentile females (n=9 scaled) and 50th percentile males (n=9)

Rear-Seat Impact Responses

Figure 32 shows the shoulder belt forces and maximal chest deflections at the mid-sternum in rear-seat impact condition for all the 50th percentile female and male HBMs. HBMs with ribcage (bottom row of the Figure) and pelvis (top row of the Figure) geometry variations are shown separately. Overall, the shoulder belt forces exhibit minimal variation. However, the maximal chest deflections show significant variation in HBMs with ribcage geometry variations. Specifically, deeper ribcages are associated with great chest deflections.

Figures 33 to 36 show the body excursions in the head, and hip in X and Z directions. Again, HBMs with pelvis (Figures 33 and 34) and ribcage (Figures 35 and 36) geometry variations are shown separately. Interestingly, head excursions in both X and Z directions, along with hip, and shoulder excursions in the X direction, present limited variation. In contrast, hip and shoulder excursions in the Z direction display greater variation, though still significantly smaller than the variations in PMHS data.

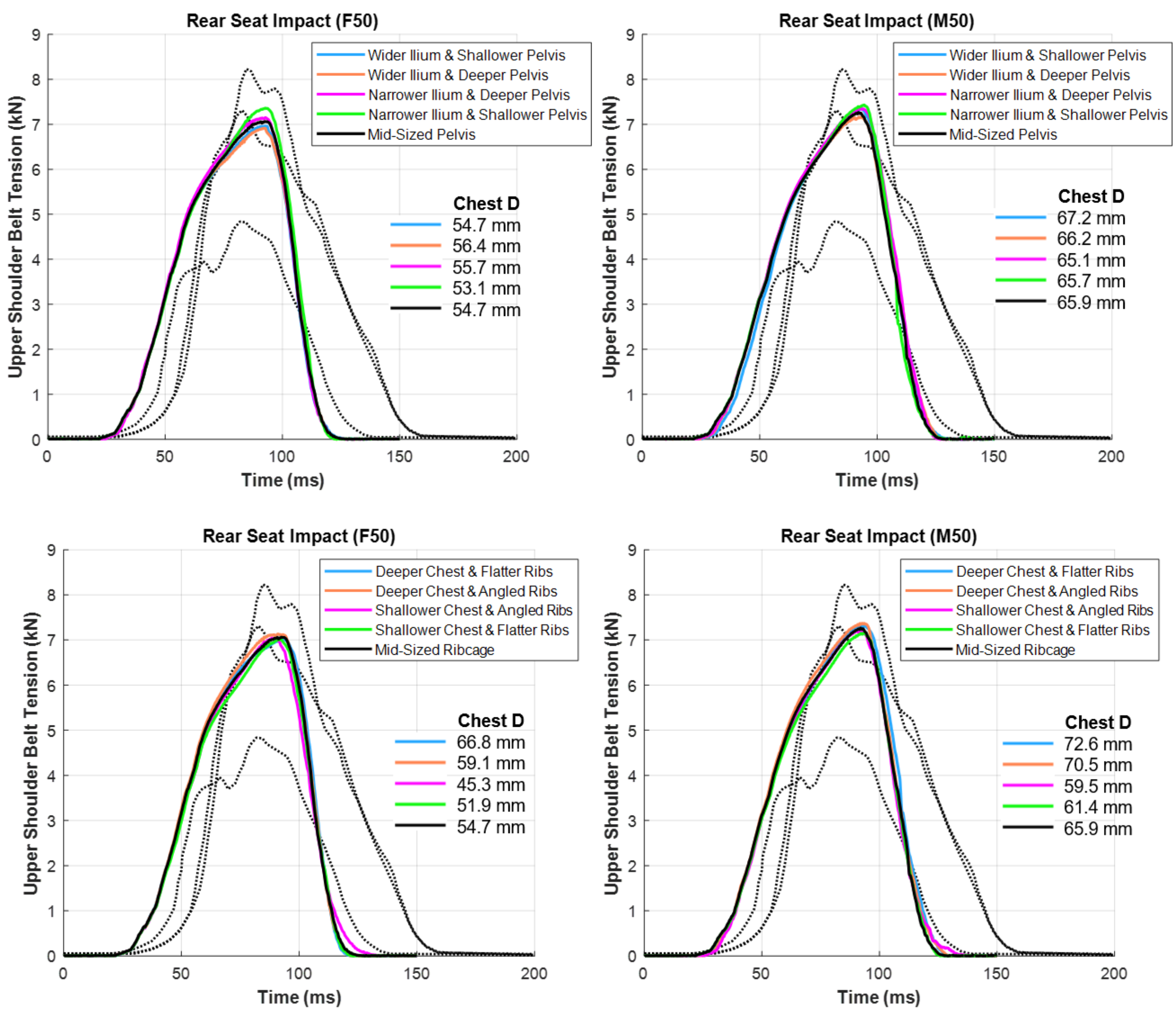

Figure 32. Shoulder belt forces in rear-seat impact condition for 50th percentile females (n=9 on the left) and 50th percentile males (n=9 on the right)

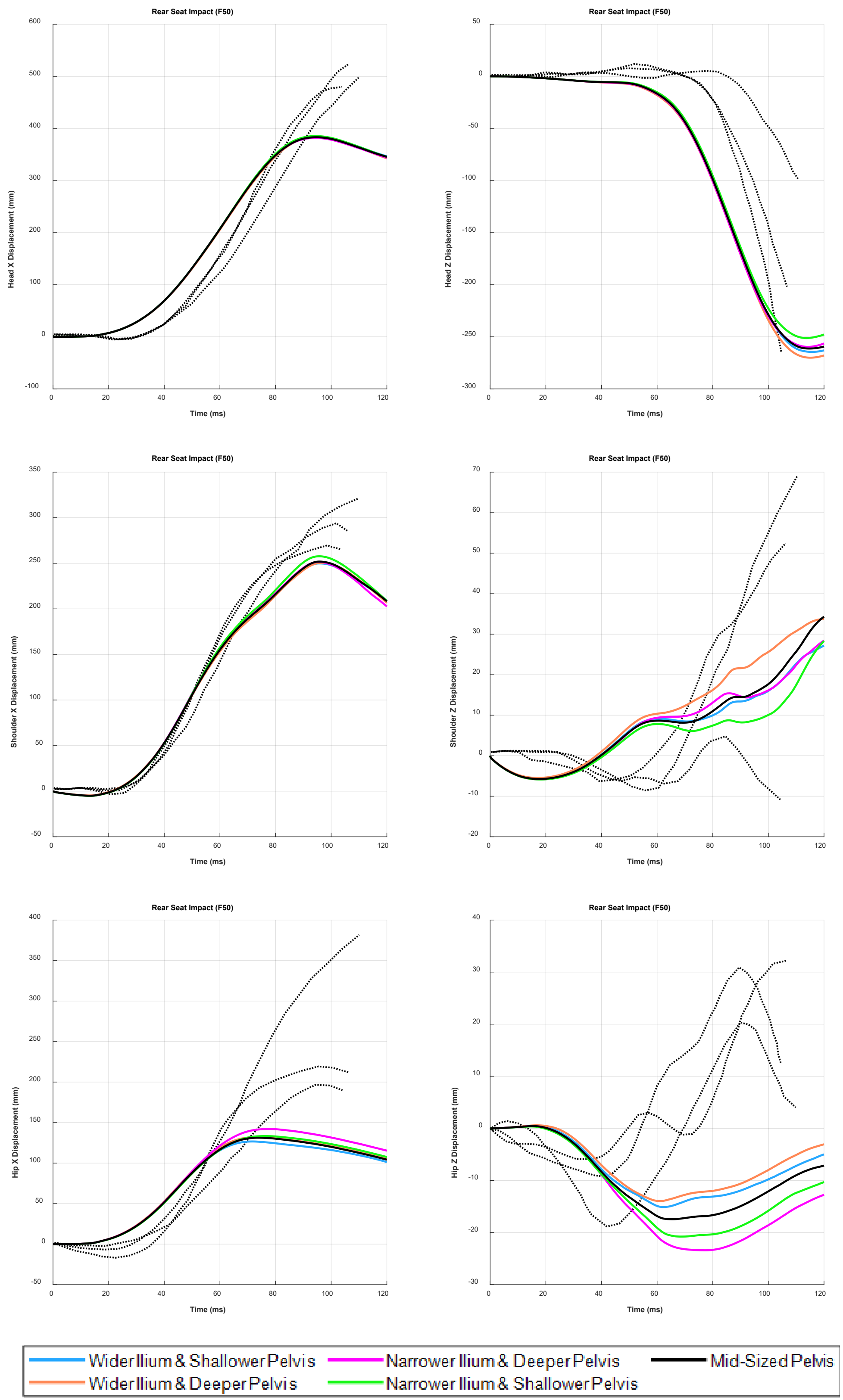

Figure 33. Body excursions in rear-seat impact condition for 50th percentile females (n=5) with varied pelvis geometry

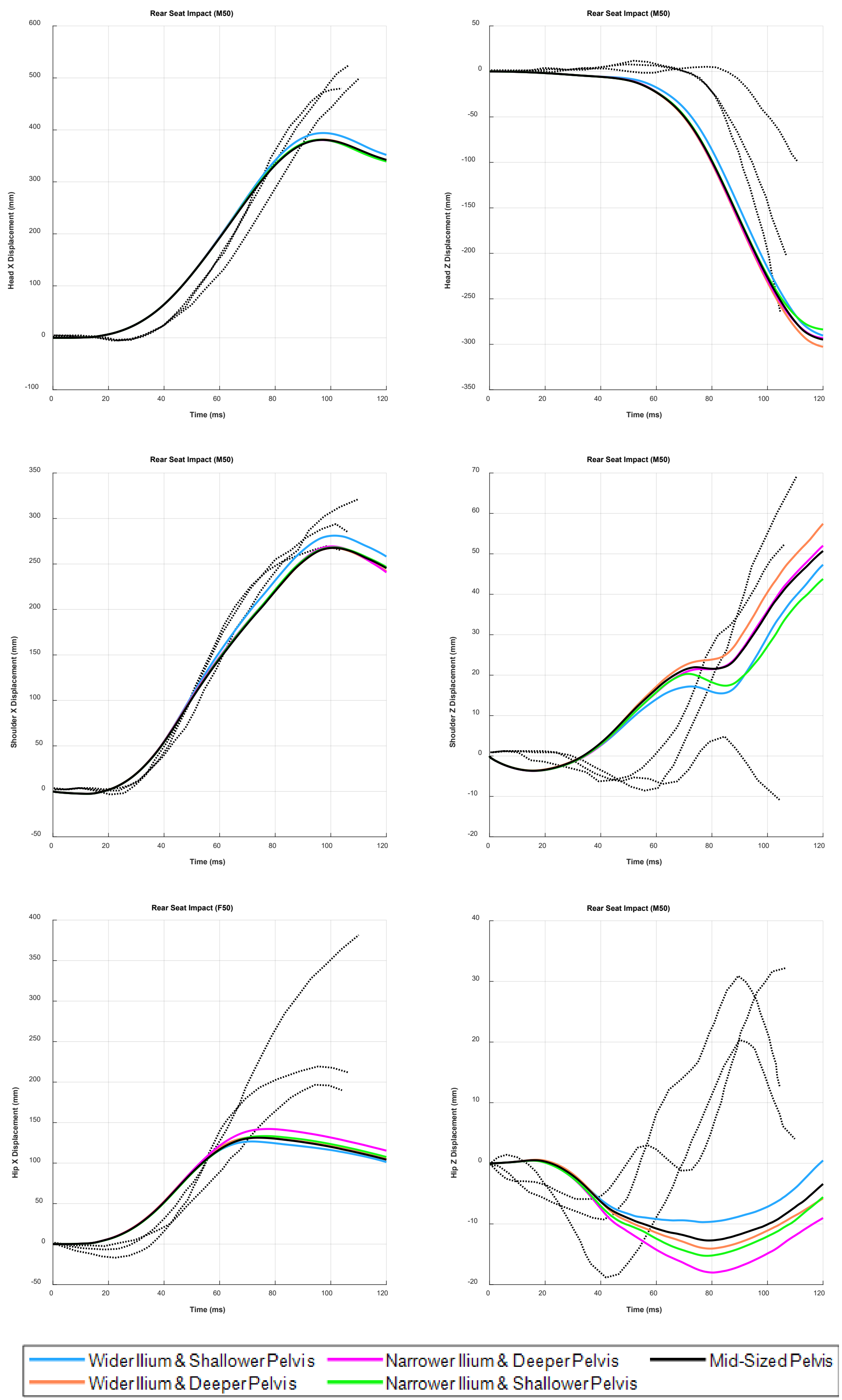

Figure 34. Body excursions in rear-seat impact condition for 50th percentile males (n=5) with varied pelvis geometry

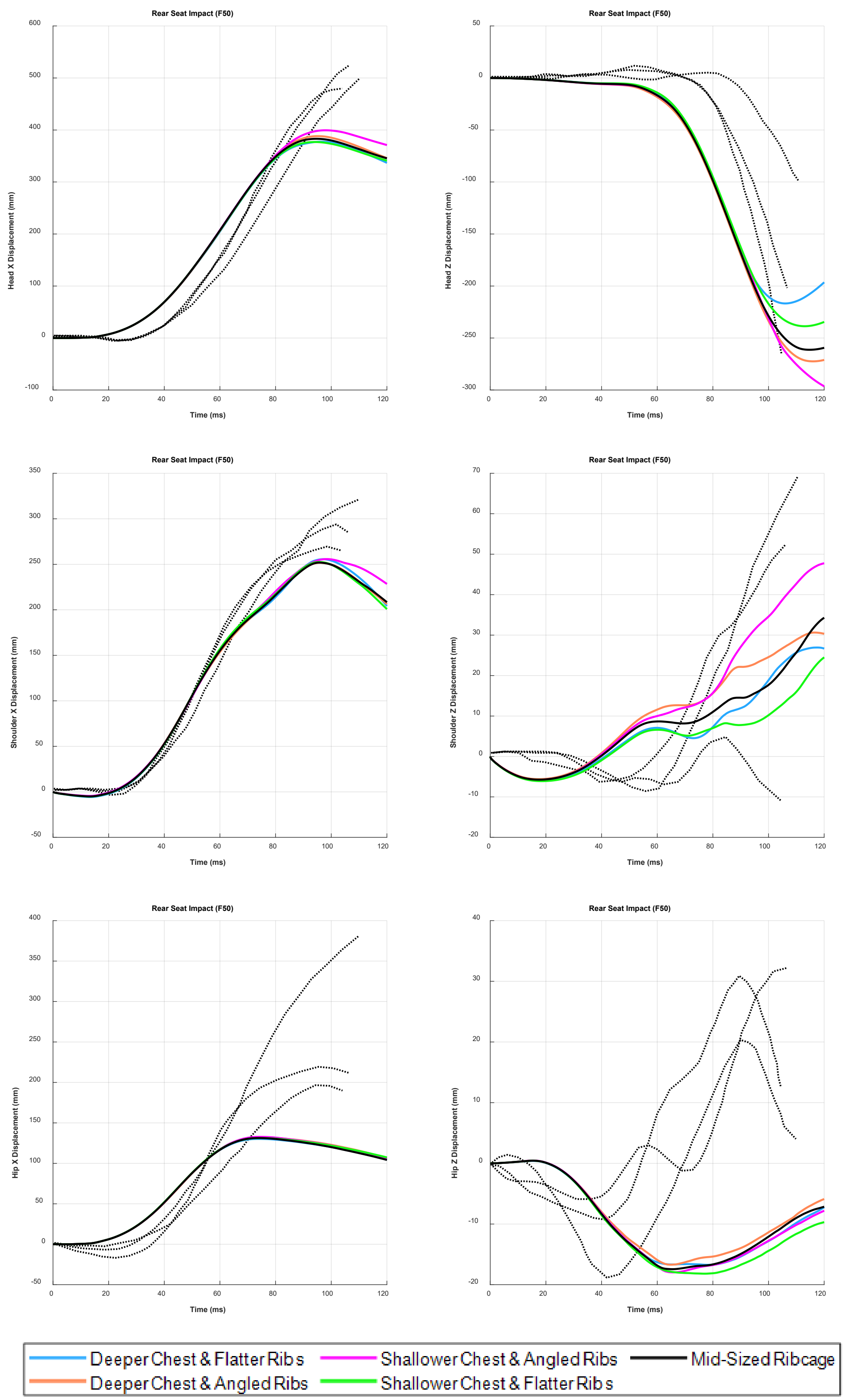

Figure 35. Body excursions in rear-seat impact condition for 50th percentile females (n=5) with varied ribcage geometry

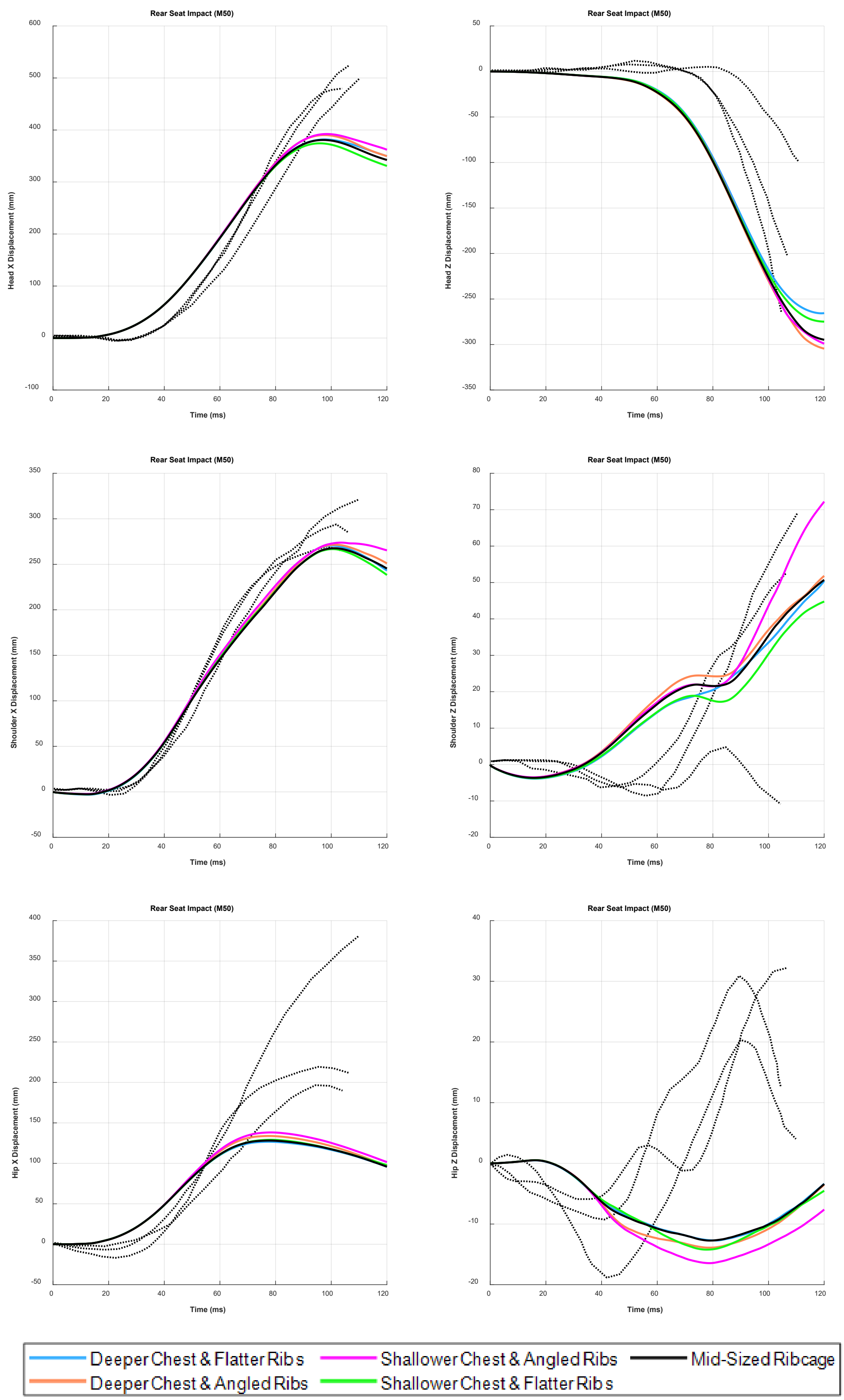

Figure 36. Body excursions in rear-seat impact condition for 50th percentile males (n=5) with varied ribcage geometry

US-NCAP Simulation Results

Figures 37 and 38 show HBM kinematics at 90 ms (around peak excursion time) and the peak head and hip excursions (mm) in the driver and front passenger locations under a US-NCAP frontal crash condition. The geometry variations do not show noticeable effects on occupant kinematics, although both head and hip excursions show some variations.

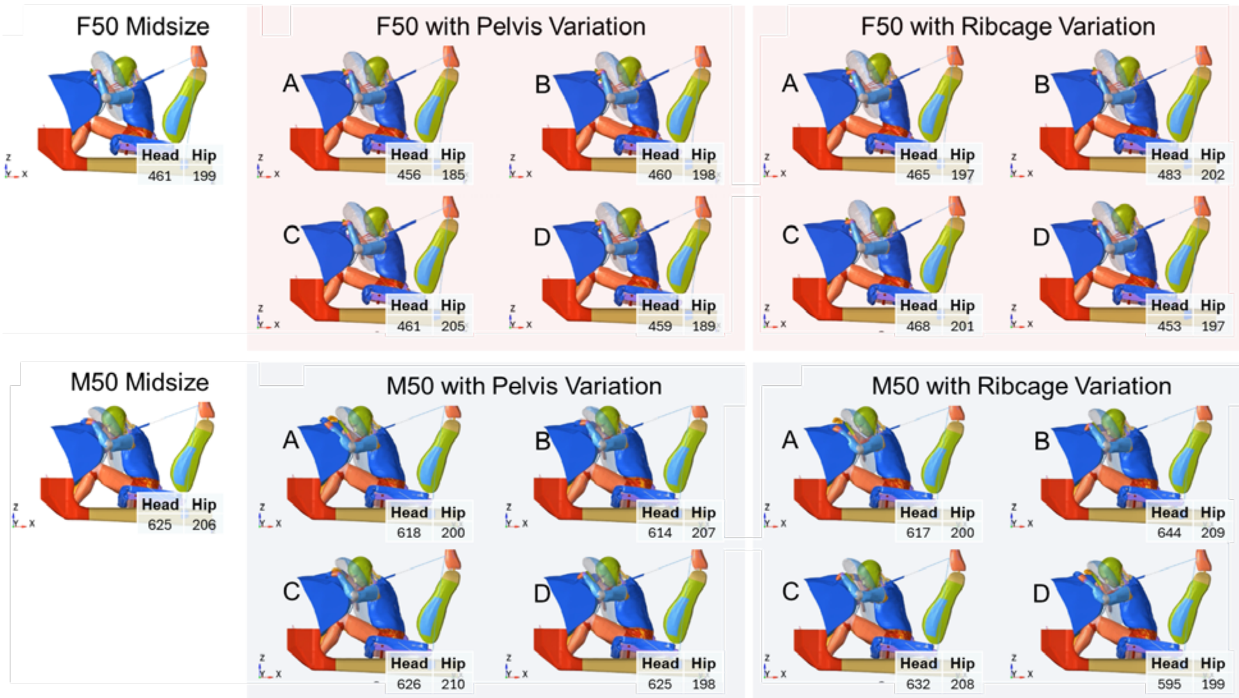

Figure 37. HBM kinematics (t=90 ms) and peak head and hip excursions (mm) in the driver position of US-NCAP frontal crash for 50th percentile females (n= 9 on the top) and 50th percentile males (n=9 at the bottom).

For pelvis, A: Wider & Shallower Pelvis, B: Wider & Deeper Pelvis, C: Narrower & Deeper Pelvis, and D: Narrower & Shallower Pelvis. For ribcage, A: Deeper Chest & Flatter Ribs, B: Deeper Chest & Angled Ribs, C: Shallower Chest & Angled Ribs, and D: Shallower Chest & Flatter Ribs.

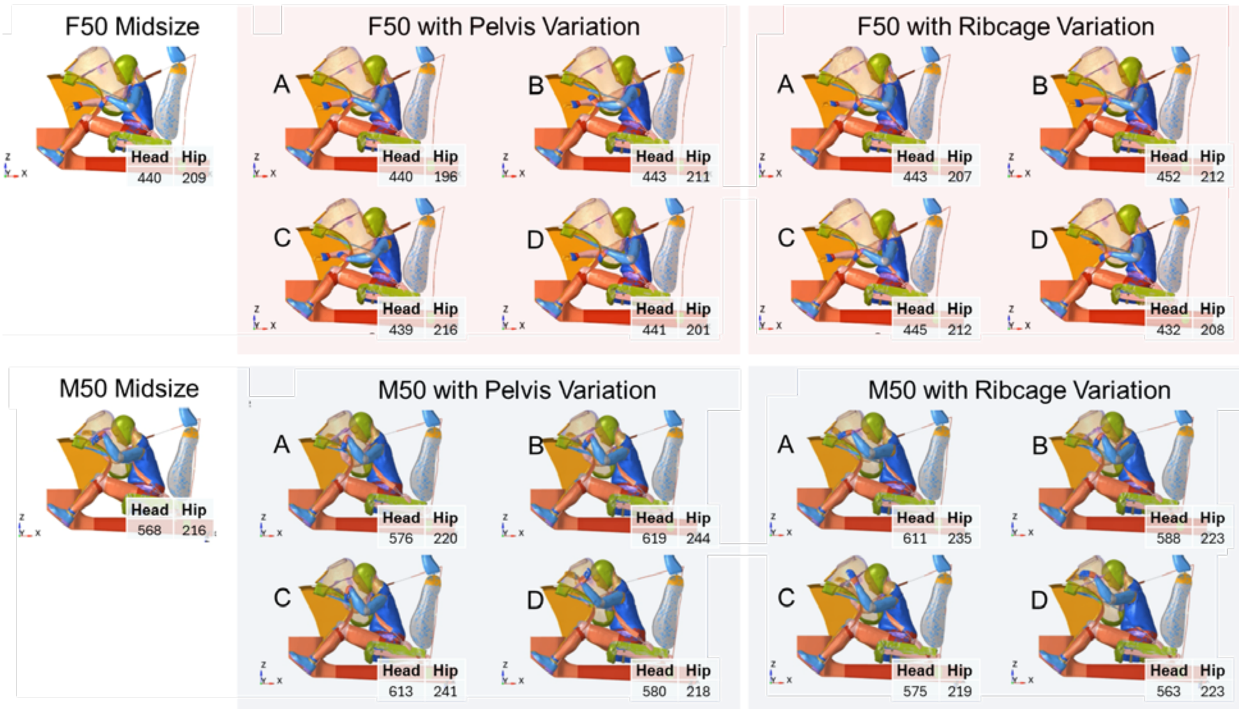

Figure 38. HBM kinematics (t=90 ms) and peak head and hip excursions (mm) in the front passenger position of US-NCAP frontal crash for 50th percentile females (n=9 on the top) and 50th percentile males (n=9 at the bottom).

For pelvis, A: Wider & Shallower Pelvis, B: Wider & Deeper Pelvis, C: Narrower & Deeper Pelvis, and D: Narrower & Shallower Pelvis. For ribcage, A: Deeper Chest & Flatter Ribs, B: Deeper Chest & Angled Ribs, C: Shallower Chest & Angled Ribs, and D: Shallower Chest & Flatter Ribs.

Table 5 shows the predicted injury risks for all F50 and M50 HBMs seated in the driver position under the US-NCAP frontal crash condition. For F50 HBMs, injury risks across most body regions are highly consistent, except for the chest, where ribcage geometry variations lead to chest injury risks ranging from 48.7 to 58.1 percent. Similarly, the M50 HBMs also show substantial variation in chest injury risk ranging from 32.8 to 50.8 percent due to ribcage geometry variation. Unlike the F50 HBMs, M50 HBMs also exhibit notable variation in brain injury risks ranging from 2.2 to 27.8 percent as a result of ribcage geometry variation and ranging from 13.1 to 22.7 percent as a result of pelvis geometry variation. Additionally, one M50 HBM with a deeper chest and angled ribs penetrated through the airbag, leading to a significantly higher head injury risk of 68.1 percent. However, it should be noted that the IP in the RAV4 model is currently defined as rigid, which may have artificially inflated the predicted head injury risk.

It may seem counterintuitive that variations in pelvis geometry could lead to significant differences in brain injury risk for M50 HBMs. However, a further comparison of the kinematics from two simulations, one using an M50 HBM with a wider and deeper pelvis and the other with a narrower and deeper pelvis, revealed that the HBM with the wider pelvis had better engagement with the lap belt, resulting in reduced torso excursion compared to the narrower pelvis model. This difference led to variations in BrIC values.

Table 5. Injury risks predicted by the 50th percentile female and male HBMs in the driver location under the US-NCAP frontal crash condition

HBM	Variation	Description	Head	Brain	Neck	Chest	Femur	TibiaU	TibiaL	Pjoint
F50	Pelvis	Wider & Shallower Pelvis	2.3%	0.5%	0.1%	55.8%	10.0%	6.8%	47.8%	81.1%
F50	Pelvis	Wider & Deeper Pelvis	2.3%	0.7%	0.1%	55.4%	11.6%	7.8%	52.3%	83.1%
F50*	**Pelvis**	**Midsize Pelvis**	2.3%	0.4%	0.1%	55.1%	11.3%	7.9%	51.9%	82.8%
F50	Pelvis	Narrower & Deeper Pelvis	2.1%	0.1%	0.1%	54.9%	11.3%	8.6%	52.2%	82.9%
F50	Pelvis	Narrower & Shallower Pelvis	2.0%	0.1%	0.1%	57.0%	10.1%	6.9%	45.7%	80.9%
F50	Ribcage	Deeper Chest & Flatter Ribs	2.2%	2.3%	0.1%	48.7%	11.7%	7.0%	47.3%	78.3%
F50	Ribcage	Deeper Chest & Angled Ribs	1.2%	0.0%	0.1%	52.0%	10.5%	8.9%	50.1%	80.7%
F50*	**Ribcage**	**Midsize Ribcage**	2.3%	0.4%	0.1%	55.1%	11.3%	7.9%	51.9%	82.8%
F50	Ribcage	Shallower Chest & Angled Ribs	1.5%	0.0%	0.1%	56.8%	10.9%	8.4%	52.0%	83.3%
F50	Ribcage	Shallower Chest & Flatter Ribs	2.9%	1.3%	0.1%	58.1%	11.7%	6.3%	46.0%	81.9%
M50	Pelvis	Wider & Shallower Pelvis	1.4%	17.2%	0.2%	37.3%	5.6%	3.8%	24.4%	57.6%
M50	Pelvis	Wider & Deeper Pelvis	1.0%	13.1%	0.2%	37.6%	6.3%	4.2%	28.2%	60.2%
M50*	**Pelvis**	**Midsize Pelvis**	0.9%	20.8%	0.2%	39.2%	6.4%	3.5%	22.9%	58.1%
M50	Pelvis	Narrower & Deeper Pelvis	1.0%	22.7%	0.2%	39.1%	5.8%	3.5%	25.2%	59.0%
M50	Pelvis	Narrower & Shallower Pelvis	1.3%	19.7%	0.2%	40.8%	5.1%	3.4%	23.5%	59.1%
M50	Ribcage	Deeper Chest & Flatter Ribs	1.7%	2.2%	0.1%	32.8%	5.9%	3.6%	25.0%	55.1%
M50	Ribcage	Deeper Chest & Angled Ribs	68.1%*	10.9%	0.2%	40.3%	6.5%	3.5%	23.8%	86.9%^
M50*	**Ribcage**	**Midsize Ribcage**	0.9%	20.8%	0.2%	39.2%	6.4%	3.5%	22.9%	58.1%
M50	Ribcage	Shallower Chest & Angled Ribs	0.5%	27.8%	0.3%	50.8%	6.7%	3.4%	23.5%	66.4%
M50	Ribcage	Shallower Chest & Flatter Ribs	1.2%	19.4%	0.2%	40.0%	5.9%	3.5%	24.7%	59.6%

*The F50 models with the midsize pelvis and midsized ribcage are the same model with average midsize female geometry, and the M50 models with the midsize pelvis and midsized ribcage are the same model as well. Each of them was presented twice in the table as the baseline model for better comparison.

^Head strikes through the airbag slightly, where the model may over-estimate the head injury risk.

Table 6 shows the predicted injury risks for all F50 and M50 HBMs seated in the front passenger position under the US-NCAP frontal crash condition. Compared to HBMs in the driver position, those in the front passenger position exhibited slightly greater variability in injury risks across different body regions, with ribcage geometry variations contributing more to injury risk differences than pelvis geometry variations. For example, in F50 HBMs, ribcage geometry variations resulted in head injury risks ranging from 4.9 to 12.0 percent, brain injury risks from 11.4 to 27.2 percent, chest injury risks from 60.6 to 71.4 percent, and lower tibia injury risks from 15.5 to 24.4 percent. Similarly, in M50 HBMs, ribcage geometry variations led to head injury risks from 7.3 to 12.3 percent, brain injury risks from 39.3 to 68.5 percent, and chest injury risks from 49.3 to 67.2 percent. In contrast, pelvis geometry variations had a more pronounced effect on brain injury risks for M50 HBMs, ranging from 41.7 to 75.3 percent, while their influence on injury risks in other body regions was relatively minor.

Table 6. Injury risks predicted by the 50th percentile female and male HBMs in the front passenger location under the US-NCAP frontal crash condition

HBM	Variation	Description	Head	Brain	Neck	Chest	Femur	TibiaU	TibiaL	Pjoint
F50	Pelvis	Wider & Shallower Pelvis	6.5%	16.2%	0.6%	67.8%	12.3%	3.8%	19.1%	79.6%
F50	Pelvis	Wider & Deeper Pelvis	6.9%	13.5%	0.6%	67.8%	15.8%	4.0%	22.2%	81.3%
F50*	**Pelvis**	**Midsize Pelvis**	6.5%	14.1%	0.7%	68.5%	13.6%	3.8%	21.2%	80.8%
F50	Pelvis	Narrower & Deeper Pelvis	6.7%	15.4%	0.6%	67.6%	12.9%	4.0%	20.8%	80.1%
F50	Pelvis	Narrower & Shallower Pelvis	6.3%	25.5%	0.6%	68.2%	11.4%	3.5%	17.0%	79.0%
F50	Ribcage	Deeper Chest & Flatter Ribs	7.5%	15.1%	0.3%	60.6%	12.7%	3.1%	17.0%	74.5%
F50	Ribcage	Deeper Chest & Angled Ribs	12.0%	25.0%	0.8%	67.2%	14.3%	4.3%	24.4%	82.3%
F50*	**Ribcage**	**Midsize Ribcage**	6.5%	14.1%	0.7%	68.5%	13.6%	3.8%	21.2%	80.8%
F50	Ribcage	Shallower Chest & Angled Ribs	4.9%	27.2%	0.9%	71.4%	14.3%	4.3%	23.1%	83.0%
F50	Ribcage	Shallower Chest & Flatter Ribs	7.2%	11.4%	0.6%	67.3%	12.5%	2.9%	15.5%	78.3%
M50	Pelvis	Wider & Shallower Pelvis	8.8%	41.7%	0.6%	58.3%	5.3%	3.7%	19.2%	72.1%
M50	Pelvis	Wider & Deeper Pelvis	10.4%	75.3%	2.0%	54.8%	7.9%	4.2%	21.3%	72.5%
M50*	**Pelvis**	**Midsize Pelvis**	8.7%	43.6%	0.7%	60.3%	5.5%	3.7%	22.2%	74.5%
M50	Pelvis	Narrower & Deeper Pelvis	10.2%	73.5%	2.3%	57.2%	7.0%	4.1%	20.5%	73.4%
M50	Pelvis	Narrower & Shallower Pelvis	11.4%	51.7%	0.9%	60.1%	4.6%	3.3%	17.2%	73.3%
M50	Ribcage	Deeper Chest & Flatter Ribs	12.3%	68.5%	1.1%	49.3%	7.3%	3.5%	19.8%	68.4%
M50	Ribcage	Deeper Chest & Angled Ribs	7.3%	51.8%	0.6%	59.8%	5.6%	4.0%	20.6%	73.3%
M50*	**Ribcage**	**Midsize Ribcage**	8.7%	43.6%	0.7%	60.3%	5.5%	3.7%	22.2%	74.5%
M50	Ribcage	Shallower Chest & Angled Ribs	7.5%	52.3%	0.9%	67.2%	5.6%	4.1%	21.0%	78.5%
M50	Ribcage	Shallower Chest & Flatter Ribs	8.5%	39.3%	0.5%	57.3%	5.5%	3.3%	21.9%	72.3%

*The F50 models with the midsize pelvis and midsized ribcage are the same model with average midsize female geometry, and the M50 models with the midsize pelvis and midsized ribcage are the same model as well. Each of them was presented twice in the table as the baseline model for better comparison.

Summary

This study used parametric HBMs to understand how geometric variability among individuals who have the same sex, stature, and body weight may affect the impact responses and injury outcomes, specifically focusing on the midsize male and midsize female population. We first detailed the methods of quantifying the geometric variations in skeleton and external body surface in midsize male and midsize female occupants using PCA, regression, and residual error analysis. Our findings revealed significant geometric variability in the ribcage and pelvis, whereas variations in the femur and tibia were minimal for both midsize males and females. Based on these geometric analyses, nine midsize male and nine midsize female geometry models were developed, focusing on ribcage and pelvis variations, which account for the majority of the observed geometric variability. The simplified GHBMC midsize male model was then morphed to match the predicted geometries of the 18 HBMs. Subsequently, 162 impact simulations were conducted under nine impact conditions using the morphed HBMs. Overall, the component-level impact simulations demonstrated relatively small variations in HBM impact responses among models with the same sex, stature, and body weight. However, in the US-NCAP frontal crash simulations, notable variations in injury risk were observed, especially in the front passenger position. These results suggest that geometric variability, even among HBMs with the same sex, stature, and body weight, should not be overlooked when assessing injury risks in severe frontal crashes.

This page is intentionally left blank.

References

Bouquet, R., Ramet, M., Bermond, F., Caire, Y., Talantikite, Y., Robin, S., & Voiglio, E. (1998, May 31–June 4). *Pelvis human response to lateral impact* [Research paper]. 16th International Technical Conference on the Enhanced Safety of Vehicles, Windsor, ON, Canada. https://www.researchgate.net/publication/264471598_Pelvis_human_response_to_lateral_impact

Boyle, K. J., Hu, J., Reed, M. P., & Rupp, J. D. (2024, September 11–13). *Development of parametric finite element vehicle and restraint models for occupant protection research* [Research paper]. 2024 International Research Council on Biomechanics of Injury (IRCOBI) Conference, Stockholm, Sweden. https://www.ircobi.org/wordpress/downloads/irc24/pdf-files/24137.pdf

Brynskog, E., Iraeus, J., Reed, M. P., & Davidsson, J. (2021, September 20). Predicting pelvis geometry using a morphometric model with overall anthropometric variables. *Journal of Biomechanics, 126*. https://doi.org/10.1016/j.jbiomech.2021.110633

Cavanaugh, J. M., Walilko, T. J., Malhotra, A., Zhu, Y., & King, A. I. (1990, November 4–7). *Biomechanical response and injury tolerance of the thorax in twelve sled side impacts* [Technical paper]. 34th Stapp Car Crash Conference, Orlando, Florida, United States. https://doi.org/10.4271/902307

Craig, M., Parent, D., Lee, E., Rudd, R., Takhounts, E., & Hasija, V. (2020). *Injury criteria for the THOR 50th male ATD.* National Highway Traffic Safety Administration. https://lindseyresearch.com/wp-content/uploads/2021/10/NHTSA-2020-0032-0003-Injury-Criteria-for-the-THOR-50th-Male-ATD-for-peer-review.pdf

Daniels, G. S. (1952). *The "Average Man"?* [Technical report]. Air Force Aerospace Medical Research Lab, Wright-Patterson Air Force Base, OH. https://apps.dtic.mil/sti/citations/tr/AD0010203

Forman, J., Lopez-Valdes, F., Lessley, D., Kindig, M., Kent, R., Ridella, S., & Bostrom, O. (2009, November 2–4). *Rear seat occupant safety: an investigation of a progressive force-limiting, pretensioning 3-point belt system using adult PMHS in frontal sled tests* [Technical paper]. 53rd Stapp Car Crash Conference, Savannah, Georgia, United States. https://doi.org/10.4271/2009-22-0002

Hardy, W. N., Schneider, L. W., & Rouhana, S. W. (2001, November 15). Abdominal impact response to rigid-bar, seatbelt, and airbag loading. *Stapp Car Crash Journal*, *45*, 1–32. https://doi.org/10.4271/2001-22-0001

Hu, J. (2018). Chapter 10–Parametric human modeling. In K.H. Yang (Ed.), *Basic finite element method as applied to injury biomechanics* (pp. 417–445). Academic Press. https://doi.org/10.1016/B978-0-12-809831-8.00010-6

Hu, J., Fischer, K., Schroeder, A., Boyle, K. J., Adler, A., & Reed, M. P. (2019a). *Development of oblique restraint countermeasures* (Report No. DOT HS 812 814). National Highway Traffic Safety Administration. https://doi.org/10.21949/1530185

Hu, J., Klinich, K. D., Reed, M. P., Ebert-Hamilton, S. M., & Rupp, J. D. (2014, December). Characterizing child head motions relative to vehicle rear seat compartment in motor vehicle crashes (Report No. DOT HS 812 105). National Highway Traffic Safety Administration. https://www.nhtsa.gov/sites/nhtsa.gov/files/documents/812105_characterizingchildheadmotions.pdf

Hu, J., Zhang, K., Reed, M. P., Wang, J. T., Neal, M., & Lin, C. H. (2019b). Frontal crash simulations using parametric human models representing a diverse population. *Traffic Injury Prevention, 20*(1), s97–s105. https://doi.org/10.1080/15389588.2019.1581926

Hwang, E., Hu, J., & Reed, M. P. (2019). Validating diverse human body models against side impact tests with post-mortem human subjects. *Journal of Biomechanics, 98*, Article 109444. https://doi.org/10.1016/j.jbiomech.2019.109444

Iraeus, J., & Lindquist, M. (2016). Development and validation of a generic finite element vehicle buck model for the analysis of driver rib fractures in real life nearside oblique frontal crashes. *Accident Analysis and Prevention*, *95*(A), 42–56. https://doi.org/10.1016/j.aap.2016.06.020

Klein, K. F. (2015). *Use of parametric finite element models to investigate effects of occupant characteristics on lower-extremity injuries in frontal crashes* (Publication No. 3722049) [Doctoral dissertation, University of Michigan]. ProQuest LLC. https://deepblue.lib.umich.edu/bitstreams/e81705e0-e347-40fb-ae10-daa3b8e78b5c/download

Klein, K. F., Hu, J., Reed, M. P., Hoff, C. N., & Rupp, J. D. (2015). Development and validation of statistical models of femur geometry for use with parametric finite element models. *Analysis of Biomedical Engineering, 43*, 2503–2514. https://doi.org/10.1007/s10439-015-1307-6

Koh, S. -W., Cavanaugh, J. M., Mason, M. J., Petersen, S. A., Marth, D. R., Rouhana, S. W., & Bolte, J. H. (2005, November 7–9). *Shoulder injury and response due to lateral glenohumeral joint impact: an analysis of combined data* [Technical paper]. 49th Stapp Car Crash Conference, Washington, D.C., United States. https://doi.org/10.4271/2005-22-0014

Laituri, T. R., Prasad, P., Sullivan, K., Frankstein, M., & Thomas, R. S. (2005, April 11–14). *Derivation and evaluation of a provisional, age-dependent, AIS3+ thoracic risk curve for belted adults in frontal impacts*. SAE 2005 World Congress and Exhibition, Detroit, Michigan, United States. https://doi.org/10.4271/2005-01-0297

Lebarbé, M., & Petit, P. (2012, September 12–14). New biofidelity targets for the thorax of a 50th percentile adult male in frontal impact [Technical paper]. 2012 IRCOBI Conference, Dublin, Ireland. https://www.ircobi.org/wordpress/downloads/irc12/pdf_files/89.pdf

National Highway Traffic Safety Administration. (2008). Consumer Information; New Car Assessment Program - Final Decision Notice, Department of Transportation, Vol. 73, No. 134.

Neathery, R. F. (1974). Analysis of chest impact response data and scaled performance recommendations. *SAE Transactions, 83*(4), 3763-3779. https://www.jstor.org/stable/i40198794

Park, B.-K. D., Jones, M. L. H., Ebert, S., & Reed, M. P. (2022). A parametric modeling of adult body shape in a supported seated posture including effects of age. *Ergonomics 65*(6), 795-803. https://doi.org/10.1080/00140139.2021.1992020

Reed, M. P., Jones, M. L. (2017). *A parametric model of cervical spine geometry and posture a parametric model of cervical spine geometry and posture*. University of Michigan Transportation Research Institute. https://deepblue.lib.umich.edu/bitstreams/ab9bc2df-3d5e-480d-a7d0-08c4061e3127/download

Takhounts, E. G., Craig, M. J., Moorhouse, K., McFadden, J., & Hasija, V. (2013). Development of brain injury criteria (BrIC). *Stapp Car Crash Journal*, *57*, 243–266. https://doi.org/10.4271/2013-22-0010

Tang, J., Zhou, Q., Nie, B., & Hu, J. (2020). Obesity effects on pedestrian lower extremity injuries in vehicle-to-pedestrian impacts: A numerical investigation using human body models. *Traffic Injury Prevention, 21,* 569-574. https://doi.org/10.1080/15389588.2020.1821195

Tang, L., Hu, Z., Lin, Y.S., & Hu, J. (2022). A statistical lumbar spine geometry model accounting for variations by age, sex, stature, and body mass index. *Journal of Biomechanics, 130,* Article 110821. https://doi.org/10.1016/j.jbiomech.2021.110821

Viano, D. C. (1989). *Biomechanical responses and injuries in blunt lateral impact* [Technical paper]. 33rd Stapp Car Crash Conference, Washington, D.C., United States. https://doi.org/10.4271/892432

Wang, Y., Cao, L., Bai, Z., Reed, M. P., Rupp, J. D., Hoff, C. N., Hu, J. (2016). A parametric ribcage geometry model accounting for variations among the adult population. *Journal of Biomechanics, 49*(13), 2791-2798. https://doi.org/10.1016/j.jbiomech.2016.06.020

Wei, A., Wang, J., Liu, J., Jones, M. L. H., Hu, J. (2022). A parametric head geometry model accounting for variation among adolescent and young adult populations. *Computer Methods and Programs in Biomedicine, 220*. https://doi.org/10.1016/j.cmpb.2022.106805

Zhang, K., Cao, L., Fanta, A., Reed, M. P., Neal, M., Wang, J.-T., Lin, C.-H., & Hu, J. (2017). An automated method to morph finite element whole-body human models with a wide range of stature and body shape for both men and women. *Journal of Biomechanics, 60*, 253-260. https://doi.org/10.1016/j.jbiomech.2017.06.015

DOT HS 813 836
September 2026

U.S. Department
of Transportation

National Highway
Traffic Safety
Administration

NHTSA

17001-082626-v3